NASA

Technical Memorandum 78020

Recovery of Refractivity Profiles and Pressure and Temperature Distributions in the Lower Atmosphere from Satellite-to-Satellite Radio Occultation Data

Charles W. Murray, Jr.

NOVEMBER 1977

National Aeronautics and
Space Administration

Goddard Space Flight Center
Greenbelt, Maryland 20771

TM 78020

RECOVERY OF REFRACTIVITY PROFILES AND PRESSURE AND TEMPERATURE DISTRIBUTIONS IN THE LOWER ATMOSPHERE FROM SATELLITE-TO-SATELLITE RADIO OCCULTATION DATA

Charles W. Murray, Jr.

November 1977

GODDARD SPACE FLIGHT CENTER
Greenbelt, Maryland

RECOVERY OF REFRACTIVITY PROFILES AND PRESSURE AND TEMPERATURE DISTRIBUTIONS IN THE LOWER ATMOSPHERE FROM SATELLITE-TO-SATELLITE RADIO OCCULTATION DATA

Charles W. Murray, Jr.

ABSTRACT

The advent of satellite-to-satellite tracking has provided a means for recovering atmospheric refractivity profiles and for retrieving certain atmospheric parameters such as pressure and temperature from radio occultation data. Profiles calculated in this manner might be used to monitor world-wide weather patterns.

The purpose of the present investigation is to demonstrate the feasibility of recovering these parameters from one-way range rate between two earth orbiting spacecraft during occultation of the tracking signal by the earth's lower atmosphere. One of the spacecraft, the ATS-6 (Applications Technology Satellite), is in a geostationary orbit in the equatorial plane. The other, NIMBUS-6, is in a near-circular almost polar orbit of about 1100 kilometers.

The tracking data is inverted by an integral transformation (Abel transform) to obtain a vertical refractivity profile above the point of closest approach of the ray connecting the satellites. The only restriction concerning the refractivity function is that it is spherically symmetric.

After accounting for ionospheric effects and water vapor in the lower atmosphere, either by independent measurement or regression techniques, pressure and

temperature distributions can be obtained from values of dry refractivity using the hydrostatic equation and perfect gas law.

Two methods are investigated for recovering pressure and temperature parameters. In the first method refractivity (which is proportional to density in a dry atmosphere) is numerically integrated to obtain pressure. Temperature is then calculated from pressure and dry refractivity. In the second method the parameters of a linear temperature profile with height (base temperature and lapse rate) over a given height region are solved for in the least squares sense using values of dry refractivity. Weighted apriori information (such as a standard atmospheric temperature profile or previous radiosonde or satellite radiometer measurements) can also be included. Pressure is then obtained from the temperature profile and dry refractivity at the base of the atmospheric layer.

An error analysis is performed in order to assess the sensitivity of random and bias type errors in measured range rate, satellite position and velocity, and height upon recovered parameters. Results show that recovery is much more sensitive to satellite velocity errors than to satellite position errors, in particular the position errors of the geostationary satellite ATS-6 where an error of 10 kilometers in each position component effects an error of about 0.2% in recovered refractivity. An error in the height of the geoid of 5 meters effects an error in recovered refractivity on the order of 0.10%.

An example is given demonstrating recovery of parameters from radio occultation data obtained during satellite-to-satellite tracking of NIMBUS-6 by the ATS-6 satellite. Pressure recovery by integration of dry refractivity agreed more closely with radiosonde data with a maximum deviation of about 3.5%. The least squares procedure for estimating temperature, with and without apriori information, yielded a temperature profile closer to radiosonde data with a maximum deviation of about 1.5%.

CONTENTS

ILLUSTRATIONS

RECOVERY OF REFRACTIVITY PROFILES AND PRESSURE AND TEMPERATURE DISTRIBUTIONS IN THE LOWER ATMOSPHERE FROM SATELLITE-TO-SATELLITE OCCULTATION DATA

1.0 INTRODUCTION

The advent of satellite-to-satellite tracking [1] has provided a means for recovering atmospheric refractivity profiles and retrieving certain atmospheric parameters such as temperature and pressure from radio occultation data.

Radio occultation of a tracking signal between two satellites occurs whenever the signal passes through the atmosphere (Fig. 1). When this occurs, the ray is bent. In the lower atmosphere the bending is opposite to that in the ionosphere.* In addition, the signal is delayed as it travels through the atmosphere, but advanced as it travels through the ionosphere. The first effect is due to the variation in the index of refraction across the signal path which results from changes in atmospheric temperature, pressure, and relative humidity. The second effect is due to the fact that the index of refraction is greater than unity in the lower atmosphere, but less than unity in the ionosphere (phase index of refraction). At 2 MHz which is the frequency of the carrier signal for satellite-to-satellite tracking in this analysis, the ionosphere has less of an effect than the lower atmosphere, especially for rays that pass close to the earth. Therefore, both the bending and delay along the path combine to cause

*For this analysis the lower atmosphere is less than 100 kilometers.

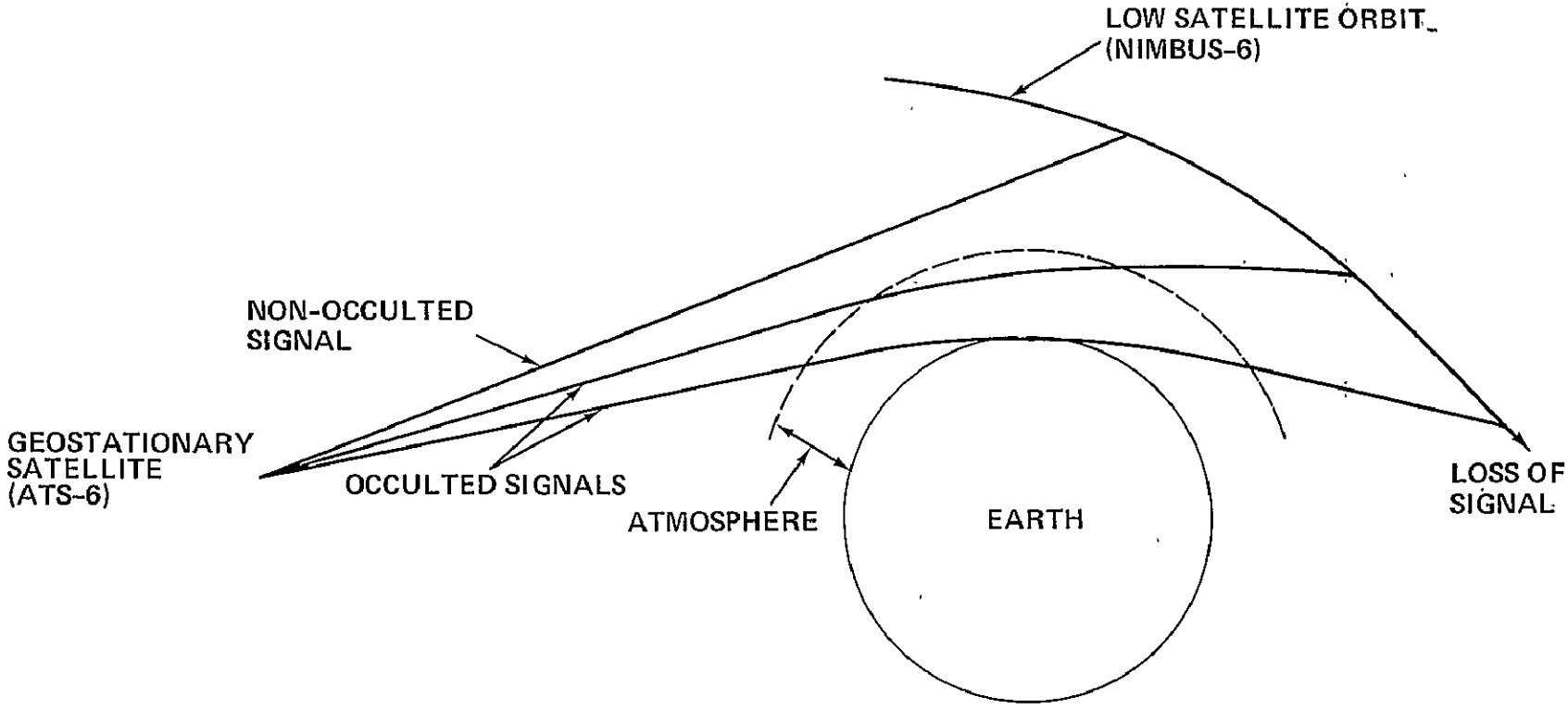

NOTE:
FIGURE IS IN PLANE CONTAINING BOTH SATELLITES AND THE CENTER OF THE EARTH.

Figure 1. Occultation Geometry

the apparent range between the two satellites to be larger than the line of sight range and the range rate along the ray path to be larger than the range rate along the line of sight.

The mathematics of profile inversion are well-documented [2] and planetary atmospheres have been studied using microwave radio occultation techniques for Mars ([3], [4], [5]) and Venus ([6], [7], [8]). Morrison, Ungar, and Lusignan [9] have proposed a system of satellites (one master satellite and a number of slave satellites) for the purpose of measuring pressure levels in the atmosphere. The satellites are placed in a common circular orbit such that the propagation path between the master and each of the slave satellites probe different levels in the atmosphere. Kliore [10] analyzed the feasibility of such a system and showed how changes in the observable quantity (phase path change) are related to changes in such meteorological parameters as density, temperature, pressure, and humidity.

The basic problem in this analysis is the following. Given the effect of the atmosphere upon one-way range rate (or equivalently doppler) between two earth-orbiting satellites (one in geostationary orbit at approximately 36,000 kilometers, the other in a low orbit of about 1100 kilometers), what is the refractivity profile which produced this effect? And, can temperature and pressure distributions be retrieved from the refractivity profile?

The answer to the first question is straightforward. With a knowledge of the position and velocity of both satellites during radio occultation,* the measured range rate can be used in an integral transformation (Abel transform) to obtain directly a vertical refractivity profile of the lower atmosphere above the point where the ray path comes closest to the earth [11]. The refractivity N is assumed to be spherically symmetric and is related to the index of refraction by

$$N = N(r) = [n(r) - 1]\, 10^{-6} \tag{1}$$

where n(r) is the index of refraction for the lower atmosphere at the geocentric radius r.

Refractivity, however, is a function of temperature, pressure, and relative humidity, and is given by ([12], pg. 7)

$$N = \frac{77.6\, P}{T} + (3.719)\, 10^5 \left(\frac{e}{T^2}\right) \tag{2}$$

where P is pressure in millibars, T is temperature in degrees Kelvin, and e is the partial pressure of the water vapor in the air (in millibars) given by ([13], pgs. 343, 353)

$$e = \frac{R_h}{100}\, (6.11)\, 10^{\frac{7.5\,(T - 273.15)}{237.3 + (T - 273.15)}} \tag{3}$$

where R_h is relative humidity in percent.

*The position and velocity of each satellite during occultation are determined from tracking data taken during nonocculted time periods using an orbit determination program. The state vectors of the satellites at a given epoch (time point close to occultation) are solved for in the program, then propagated through occultation to provide position and velocity of the satellites at the data times.

From (2) it can be seen that recovering temperature and pressure from refractivity is not as straightforward as recovering refractivity from range rate data. Account must be taken of ionospheric effects and water vapor which contributes to the wet component of refractivity, the second term on the right-hand side of (2). If these effects can be properly accounted for, either by independent measurement or regression techniques,* all that will remain will be the dry component of refractivity, the first term on the right-hand side of (2). This quantity is proportional to density in a dry atmosphere.

In this analysis two methods for obtaining temperature and pressure distributions from dry refractivity are investigated. In both cases the equation of hydrostatic equilibrium and perfect gas law are assumed to hold. In the first method dry refractivity is numerically integrated to obtain the pressure. Temperature is then obtained from pressure and dry refractivity using the first term on the right-hand side of (2). In the second method the parameters of a linear temperature profile with height in a given atmospheric layer (base temperature and lapse rate in that region) are obtained from values of dry refractivity using nonlinear least squares. Apriori information (such as a standard atmospheric temperature profile or previous radiosonde or satellite radiometer data) can also be included.

*By selecting data above a certain height (for example 5 to 7 kilometers), the water vapor effects in the lower atmosphere can be neglected. At 2MHz and for rays passing close to the earth, the change in the contribution of the ionosphere to the total path length (as well as the rate of change of path length) of the signal should be rather small. For these reasons a simple model for ionospheric density in the upper atmosphere should suffice. For rays passing higher up in the atmosphere a dual frequency system can be used to remove ionospheric effects.

Pressure is then obtained from the recovered temperature profile and the dry refractivity at the base of the layer.

The advantage of obtaining pressure by numerically integrating dry refractivity is that no assumption is made concerning the temperature structure. In a dry atmosphere refractivity is a direct measurement of density. In order to recover the pressure accurately, however, a sufficient number of points over a wide range of heights must be available for the numerical integration. If there is sufficient reason to believe that temperature is linear with height in a given region, then not as many points would be required to obtain the least squares solution for the temperature profile.

There is a similarity in the mathematical techniques of recovering temperature from dry refractivity and recovering temperature from radiation measurements, as well as in the structuring of temperature as a piecewise linear function with height. Smith [14], [15] models the lower atmospheric temperature with two lapse rates. In regard to the subject of temperature retrieval, Rodgers [16] has written an excellent comprehensive survey paper.

An advantage afforded by the geometrical configuration of the satellite orbits in this analysis (one in geostationary orbit and the other in a noncoplanar orbit) is that different pressure levels in the lower atmosphere can be probed with just one satellite pair. In addition, for a fixed inclination of the nongeostationary satellite orbit, occultations will occur at about the same latitude in both the

northern and southern hemispheres, but at varying longitudes. A system of satellites in various inclined orbits could provide latitude coverage for monitoring world-wide weather patterns.

2.0 ATS-6/NIMBUS-6 GEOMETRY

The geometry of ATS-6 and NIMBUS-6 can be seen in Figure 2 where ATS is in a near-circular geostationary orbit in the equatorial plane and NIMBUS-6 is in a near-circular orbit close to polar (approximate height of 1100 kilometers).

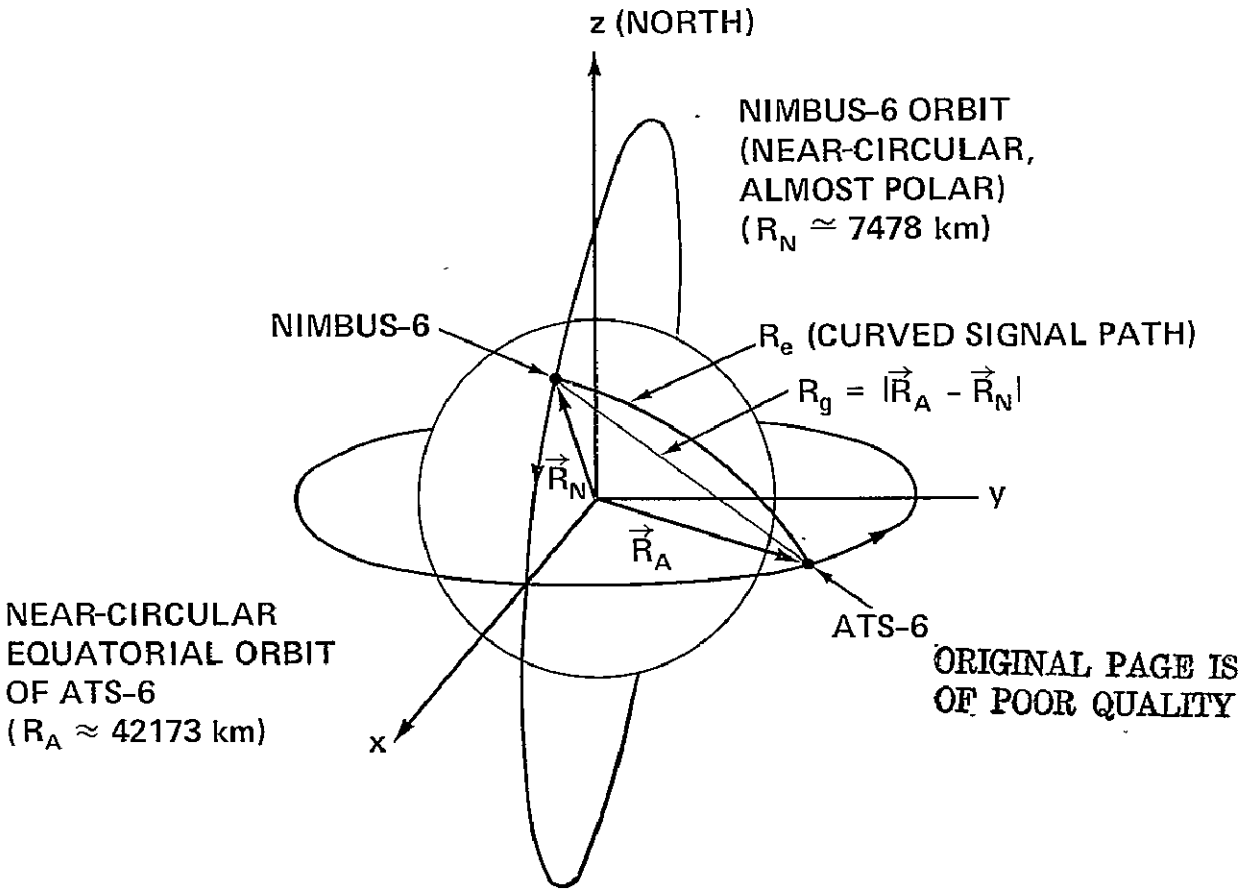

Figure 2. ATS-6/NIMBUS-6 Geometry

3.0 TRACKING MEASUREMENTS

For the ATS-6/NIMBUS-6 Tracking Experiment [1] the signal travels a 4-way path as shown in Figure 3 (from [1]). The range measurement consists of the time in seconds between a zero crossing of the ground transmitted signal (6 GHz carrier phase modulated by a 100 KHz sidetone) and a zero crossing of the ground received signal (4 GHz carrier having two subcarriers each phase modulated by the 100 KHz sidetone) after the signal has travelled from ground to ATS, to NIMBUS, back to ATS, and then to ground [1]. The range rate measurement consists of the time in seconds required to count a fixed number of cycles of the 4-way Doppler frequency plus a fixed offset frequency.

For inversion purposes the measurement consists of the one-way range rate between ATS-6 and NIMBUS-6 which is obtainable from the 4-way Doppler data.*

4.0 ATMOSPHERIC EFFECT

The atmospheric effect upon range is the difference between the electrical range along the ray path and the geometric straight line distance between the two satellites (absence of an atmosphere). The atmospheric effect upon range rate is

*The 4-way Doppler output for ATS-6 Satellite-to-Satellite tracking can be approximated by [17]

$$f_d \doteq \frac{-2f_t k}{c} [a_1 \bar{\dot{r}}_1 + a_2(\bar{\dot{r}}_1 + \bar{\dot{r}}_2)]$$

where f_d = measured average Doppler frequency
f_t = uplink frequency (6137.85 MHz)
c = speed of light
k, a_1, a_2 are scalar constants determined by equipment frequency multiplication ($k \sim .336, a_1 = 0.76, a_2 = 1.0$)
$\bar{\dot{r}}_1$ = average one-way range rate ATS to ground site
$\bar{\dot{r}}_2$ = average one-way range-rate ATS to Nimbus.

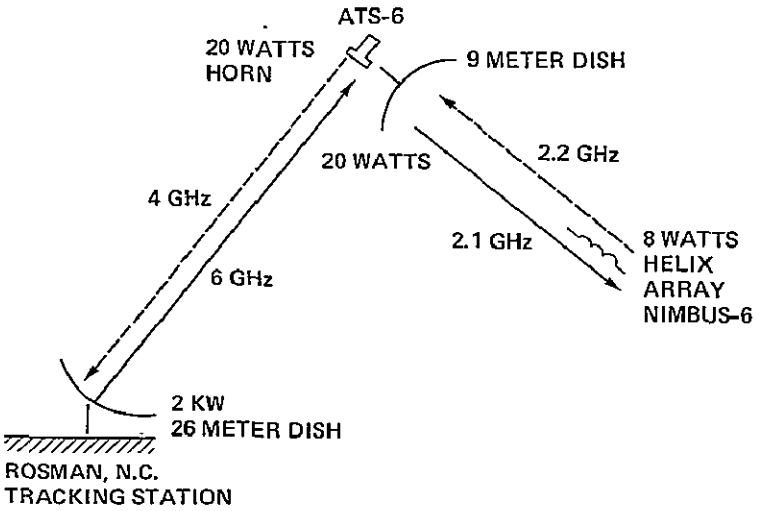

Figure 3. Tracking Measurements (from [1])

the derivative of this difference, Referring to Figure 4, the electrical distance, R_e, along the path NDCBA is given by

$$R_e = \int_N^A n(r)\, ds \tag{4}$$

where n(r) is the index of refraction for the lower atmosphere and ds is an incremental length along the ray path.

The atmospheric effect upon range and range rate is therefore

$$\Delta R = R_e - R_g \tag{5}$$

$$\Delta \dot{R} = \dot{R}_e - \dot{R}_g \tag{6}$$

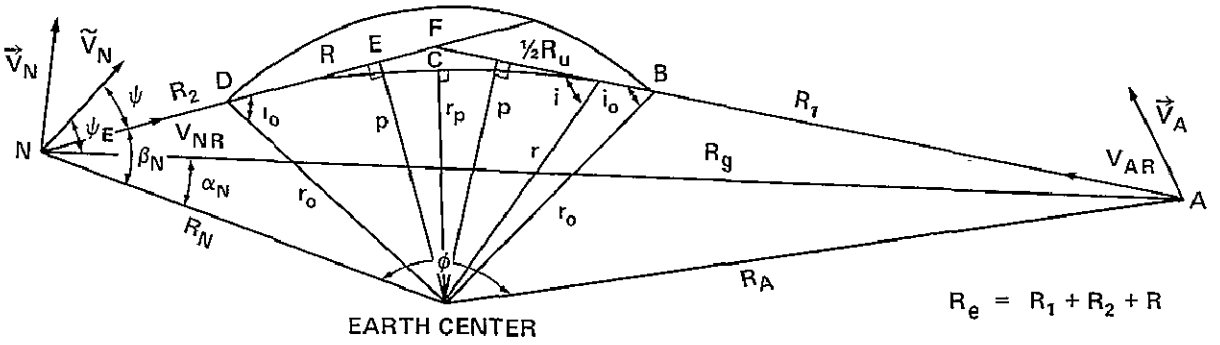

Figure 4. Ray Path Geometry

An example of the atmospheric effect upon range rate for an actual ATS-6/ NIMBUS-6 occultation pass on 15 April 1976 can be seen in Figure 5.

5.0 HERGLOTZ-WIECHERT INVERSION TECHNIQUE

This technique was originally used to determine velocity-depth profiles in the earth from the travel times of seismic waves between known positions of a source and a receiver located on the earth's surface. It has been adapted for the radio occultation problem by Phinney and Anderson [11] (see Appendix). As used here the technique provides a direct means for transforming satellite-to-satellite tracking data obtained during occultation into a profile of refractive index versus radius.

The data used in the radio occultation problem is one-way range rate between the two satellites (obtainable from the 4-way Doppler data described in Section 3.0). The method requires as input two different range rate residuals. One residual is used to determine the angle between the ray path and the radius vector of each satellite which is necessary to determine the impact parameter (Section 6.0). The other residual is used in the integral inversion formula to determine the refractive index at the minimum probing distance.

The main advantage of the Herglotz-Wiechert method compared to, say, a model fitting approach, is that the only assumption made concerning the analytical form of the refractivity is that it is spherically symmetric. Thus, no modelling errors are introduced.

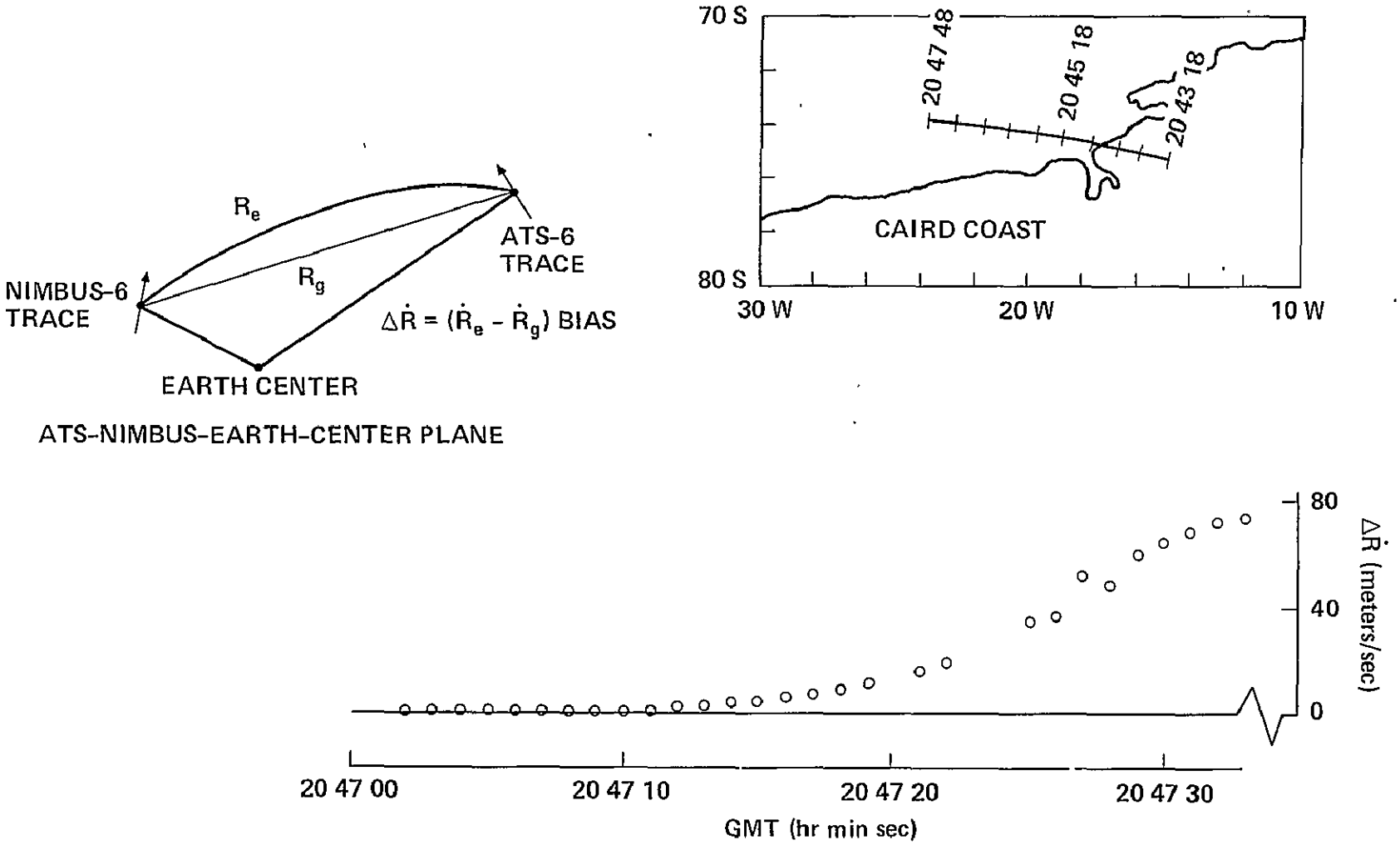

Figure 5. Radio Occultation Effect on One-way Range Rate Between ATS-6 and NIMBUS-6 (15 April 1976)

Referring to Figure 4 and following Phinney and Anderson, let r_o be the radius which defines the outer limit of the lower atmosphere (for $r \geqslant r_o$ the index of refraction is unity). A ray parameter, p, called the impact parameter of the ray, is defined as

$$p = n(r)\, r \sin i \tag{7}$$

where n(r) is the index of refraction at the radius r and i is the angle of incidence between the tangent to the ray path and the radius vector.

By Snell's law p is a constant along a ray, and in the absence of an atmosphere, is the radius of closest approach of the ray. With an atmosphere present p is perpendicular to the ray asymptote. We can also write

$$p = r_o \sin i_o = n_p r_p \tag{8}$$

where the subscript p refers to the turning point of the ray.

Define a new variable η

$$\eta = n(r)\, r = \frac{p}{\sin i} \tag{9}$$

which equals r_o when $r = r_o$ and p when $r = r_p$. The electrical range along the ray path between points B and D (which is proportional to the total phase shift at the carrier frequency) can then be expressed as a function of p

$$R(p) = 2\int_B^D n\,ds = 2\int_p^{r_o} \left(\frac{\eta^2}{r}\right) (\eta^2 - p^2)^{-1/2} \left(\frac{dr}{d\eta}\right) d\eta \tag{10}$$

where ds is an increment along the ray path.

But, the range along the ray path between B and D can be written as the sum of the range in the absence of an atmosphere, R_u, plus the range residual due to an atmosphere, R_a.

$$R = R_u + R_a \tag{11}$$

where $R_u = 2p\cot i_o$.

Using (7) through (11) and the Abel transform (see Appendix), the refractive index n_p at the minimum probing radius r_p is given by

$$n_p = \exp\left[-\frac{1}{\pi}\int_{\eta}^{r_o} \cosh^{-1}\left(\frac{p}{\eta}\right)\left(\frac{1}{p}\right)\left(\frac{dR_a}{dp}\right) dp\right] \tag{12}$$

Using (4) and the fact that the ray paths from B and D to the satellites are straight lines (ionospheric bending is negligible), R_a can be written as

$$\begin{aligned} R_a &= \int_N^A n(r)\, ds - \sqrt{R_A^2 - p^2} - \sqrt{R_N^2 - p^2} \\ &= R_e - \sqrt{R_A^2 - p^2} - \sqrt{R_N^2 - p^2} \end{aligned} \tag{13}$$

Differentiating (13) with respect to p gives the residual dR_a/dp in terms of the measured one-way range rate $\dot{R}_e$ between the satellites

$$\frac{dR_a}{dp} = \dot{R}_e\left(\frac{dt}{dp}\right) + p\left[\frac{1}{\sqrt{R_A^2 - p^2}} + \frac{1}{\sqrt{R_N^2 - p^2}}\right] \tag{14}$$

The integration in (12) is carried out numerically using Gaussian quadrature. In order to use (14) in the integrand of (12), it is necessary to determine p as a function of t. For this purpose a least squares polynomial is fit to t versus p and dt/dp obtained from the polynomial.

Refractivity is obtained using η_p in equation (1).

6.0 DETERMINATION OF IMPACT PARAMETER

The impact parameter p can be obtained iteratively using as input the ephemeris of both satellites and a range rate residual [18].

In Figure 4, which is in the plane containing both satellites and the center of the earth, the angle ψ is given by

$$\cos \psi = \frac{V_{NR}}{|\tilde{V}_N|} \tag{15}$$

where $\tilde{V}_N$ is the low satellite velocity vector $\vec{V}_N$ projected onto the plane of both satellites and the earth center, and V_{NR} is the projection of $\vec{V}_N$ along the ray path.

The measured range rate $\dot{R}_e$ can be expressed as

$$\dot{R}_e = V_{NR} + V_{AR} \tag{16}$$

where V_{AR} is the projection of the high altitude satellite velocity vector along the ray path (the dot product of the velocity vector with a unit vector along the ray path at the satellite and directed away from the low satellite) and V_{NR} is similarly defined for the low satellite.

Combining (15) and (16) we have

$$\psi = \cos^{-1}\left[\frac{\dot{R}_e - V_{AR}}{|\tilde{V}_N|}\right] \tag{17}$$

The quantity $(\dot{R}_e - V_{AR})$ in (17) is a range rate residual.

The angle β_N is given by

$$\beta_N = \alpha_N + \psi_E + \psi \tag{18}$$

where ψ_E is the angle between $\tilde{V}_N$ and the line of sight and α_N is the angle between the radius vector of the low satellite R_N and the line of sight. Both these angles are determined from the ephemeris of the satellites.

The impact parameter is given by

$$p = R_N \sin\beta_N \tag{19}$$

The iteration proceeds as follows. The projection of the high satellite velocity vector along the line of sight is input as a first guess for V_{AR} in (17) and the angle ψ calculated using the measured range rate and $|\tilde{V}_N|$ ($|\tilde{V}_N|$ can be determined from the position and velocity of the satellites). Next β_N is obtained from (18) and used in (19) to determine a value for p. Using this value for p and R_A (radius vector of the high satellite) and the ephemeris, a new value for V_{AR} is obtained which is then input to (17). The process is continued until convergence is reached.

From the above it is seen that two range rate residuals are required as input in the Herglotz-Wiechert inversion technique. The residual ($\dot{R}_e - V_{AR}$) is used in (17) to obtain the impact parameter p iteratively, while the other residual dR_a/dp, given by (14), is used in the integral transformation of (12) to obtain the index of refraction n_p at the minimum probing radius r_p.

7.0 IONOSPHERIC EFFECTS

At S-band frequencies (2 GHz carrier tracking signal between ATS and NIMBUS) and particularly for rays passing close to the earth, the effects of the ionosphere upon range and range rate are small compared to the effects of the lower atmosphere [19]. The way in which the ionosphere enters into the occultation calculations is in the computation of the path length of the signal through that region (100 kilometers to 1000 kilometers). For rays close to the earth's surface, the change in the contribution of the ionosphere to the total path length is small. Its effect upon range rate, therefore, should be negligible. Figure 6 shows the effects of the lower atmosphere and ionosphere upon range, range rate, and bending angle for an assumed exponential model for lower atmospheric refractivity and a Chapman model for the electron density in the ionosphere with parameters corresponding to a total electron content of 10^{17} electrons/meter^2.

The exponential refractivity is given by

$$N_T = N_o \exp(-h/H_T) = (n_T - 1)10^6 \qquad (20)$$

Figure 6. Comparison of Lower Atmospheric and Ionospheric Effects on Range, Range Rate, and Bending Angle

with $N_o = 330.3$

$H_T = 6.6$ kilometers (scale height)

n_T = index of refraction

h = height in kilometers

The Chapman model used in the analysis is given by

$$N_e = N_{max} \exp\left[\frac{1}{2}(1 - z - e^{-z})\right] \tag{21}$$

with $N_{max} = (0.3098) \cdot 10^{12}$ electrons/meter^3

$z = (h - h_m)/H_I$

$h_m = 300.73$ kilometers (height of maximum electron content)

$H_I = 78.11$ kilometers (scale height)

h = height in kilometers

Since the basic measurement involved in satellite-to-satellite tracking is the doppler shift of the tracking signal, the phase index of refraction is used for ray tracing through the ionosphere, and the refractivity is given by [20]

$$N_I = -\left[\frac{40.3\, N_e(h)}{f^2}\right] 10^6$$

$$(n_I - 1) \cdot 10^6 \tag{22}$$

with n_I = phase index of refraction

$f = 2$ GHz

Since the ionosphere is a dispersive medium, a distinction must be made between group and phase velocities and group and phase indices of refraction. The lower atmosphere, however, is non-dispersive. Therefore phase and group velocities are the same and phase and group indices of refraction are the same.

The curves in Figure 6 were obtained by ray tracing through the atmosphere to both satellites using (20) and (22) and the geometry of Figure 4. The range error, equation (5), was obtained using

$$R_e = R_1 + R_2 + 2\int_{r_p}^{r_o} \frac{n\, dr}{\sqrt{1-(n_p r_p/nr)^2}} \tag{23}$$

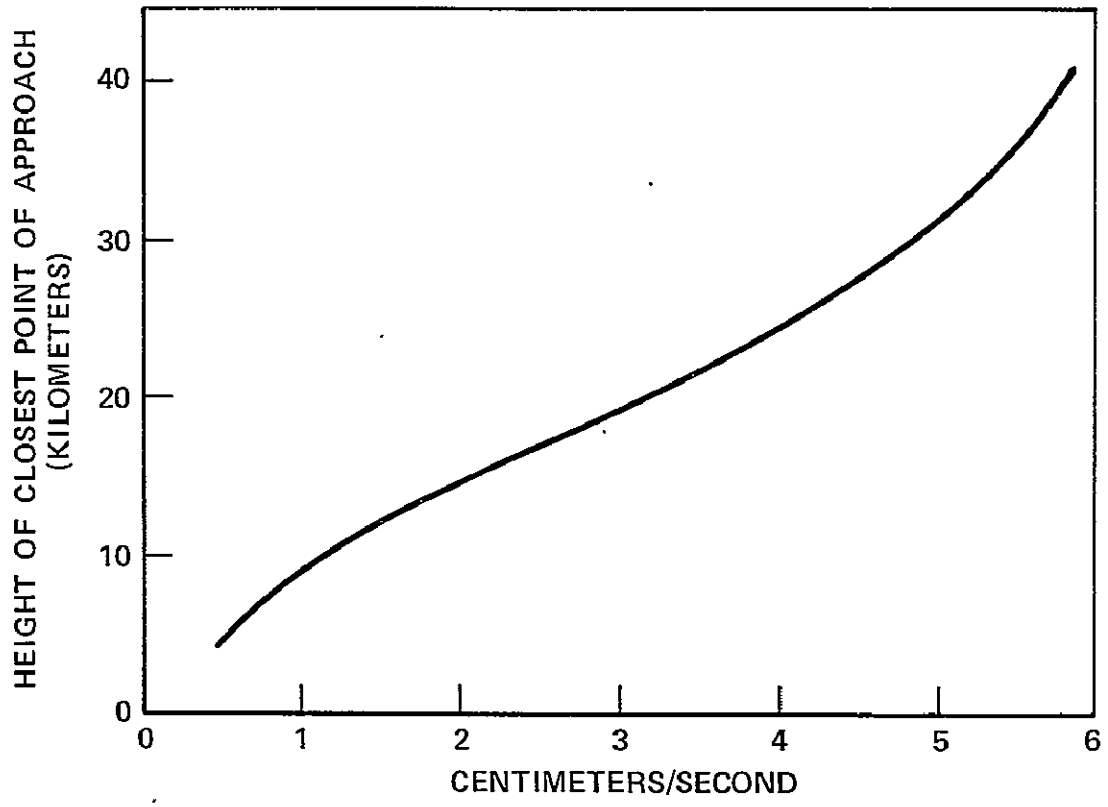

Figure 7. Ionospheric Range Rate Error for an Actual Ephemeris

where R_1 and R_2 are linear segments, and the integral on the right side of (23) is obtained from (1) and Snell's law for a spherically stratified medium.

$$n\, r \cos\theta = n_p\, r_p \tag{24}$$

where θ is the local elevation angle of the ray at the radius r, and n is obtained from (20) when ray tracing through the lower atmosphere and (22) when ray tracing through the ionosphere.

For the lower atmosphere r_o is 100 kilometers and for the ionosphere r_o is 1000 kilometers (the height of NIMBUS in this analysis). Therefore, for ray tracing with the ionospheric model, R_2 is zero.

The bending angle τ is given by [21]

$$\tau_{1,2} = -\int_{n_1}^{n_2} \cot\theta \, \frac{dn}{n} \tag{25}$$

or using (1) and (24)

$$\tau = -2\, n_p r_p \cdot 10^{-6} \int_{r_p}^{r_o} \frac{(dN/dr)\, dr}{n^2 r \sqrt{1 - (n_p r_p / nr)^2}} \tag{26}$$

where n and N are obtained from either (20) or (22)

The $\Delta\dot{R}$ curves in Figure 6 were obtained from the relation

$$\Delta\dot{R} = \frac{d\Delta R}{dr} \cdot \frac{dr}{d\phi} \cdot \frac{d\phi}{dt} \tag{27}$$

where the rates $d\Delta R/dr$ and $dr/d\phi$ were calculated in a ray trace computer program and the angle ϕ is the total central angle subtended (Fig. 4). The rate

$d\phi/dt$ was taken to be 0.001 radians/second which is the angular velocity of the NIMBUS satellite at an altitude of 1000 kilometers. This value represents an upper bound for the rate of change of the central angle (in the plane of both satellites and the center of the earth) given the geometric configuration of the ATS and NIMBUS orbits. The central angle will vary with time and be less than this value.

It can be seen from Figure 6 that the effects of the ionosphere are negligible in comparison with the effects of the lower atmosphere. Lower atmospheric bending at the surface is on the order of 1.5 degrees compared with ionospheric bending of about 0.5 millidegrees. It is mainly the bending angle τ which contributes to the large lower atmospheric range error of approximately 1.7 kilometers. Compare this with an ionospheric range error at the surface of about -6 meters.

The primary effect of interest in this analysis is the range rate error which is on the order of 100 meters/second for the lower atmosphere, but only a few centimeters/second for the ionosphere. This latter follows from the fact that the ionospheric range error is nearly constant over the range of interest. These ionospheric effects are for an electron content of 10^{17} electrons/meter^2. Since this quantity typically varies between 10^{16} and 10^{18} electrons/meter^2, the range rate effect should vary between about 0.3 centimeters/second and 30 centimeters/second.

In order to further investigate the effect of the ionosphere upon range rate, an actual ephemeris of the ATS-6 and NIMBUS-6 satellites was used (15 April 1976) along with the same ionospheric density model and lower atmospheric exponential refractivity model. N_{max}, however, was taken to be $0.42485 \cdot 10^{12}$ electrons/meter^3 (corresponding to a total electron content of about $1.4 \cdot 10^{17}$ electrons/meter^2). Rays linking the two satellites were traced with and without the ionospheric model included, and the range rate along the ray path obtained by dotting the respective velocity vectors onto unit vectors along the ray path at each satellite and summing the result. The difference between the range rates as a function of the height of closest point of approach of the ray was then obtained. The results can be seen in Figure 7. The maximum effect is on the order of about 6 centimeters/second.

It can be concluded from the above that ionospheric effects upon range rate are negligible for the frequencies involved here and for rays which pass close to the earth.

At higher altitudes a simple model for ionospheric density, such as the Chapman model indicated in (22) should suffice for removing these effects or they could be removed by employing a dual-frequency system.

If the purpose of our investigation were to recover ionospheric densities, then we would only be interested in rays passing through the ionosphere and not the lower atmosphere. In this case the situation would be reversed and ionospheric effects would be much greater than lower atmospheric effects [19].

8.0 RECOVERY OF PRESSURE AND TEMPERATURE FROM REFRACTIVITY

In this section it is assumed that the effects of the ionosphere and water vapor in the atmosphere have been removed from the recovered refractivity (either by regression techniques using some assumed model or by independent measurement). Thus, all that remains is the dry refractivity N_d, a quantity directly proportional to density. From (2)

$$N_d = \frac{77.6\,P}{T} \tag{28}$$

where P is pressure in millibars and T is temperature in degrees Kelvin.

Two methods are described for calculating temperature and pressure parameters from dry refractivity. In both methods it is assumed that hydrostatic equilibrium and the perfect gas law hold. In the first method the dry refractivity is numerically integrated to obtain pressure directly [22]. Temperature is then determined from N_d and P using (28). The second method involves solving for a base temperature T_o and temperature lapse rate β in a given atmospheric layer using values of dry refractivity in a least squares sense (weighted apriori information can be included). Pressure can then be calculated from the dry refractivity at the base of the atmospheric layer and the temperature profile. In this method it is assumed that temperature is a linear function of height.

Pressure by Integration of Dry Refractivity

The hydrostatic equation is [23]

$$dP = -\rho g(h)dh \tag{29}$$

where ρ is the density of dry air and g(h), the acceleration of gravity, is a

function of the geometric height h* ([24], pg. 217).

The perfect gas law is

$$\bar{\rho} = \frac{MP}{RT_v} \tag{30}$$

where M = the apparent molecular weight of dry air = 28.966 ([24], p. 289)

R = universal gas constant = 8.31436 joules $(°K\,mole)^{-1}$ ([24], p. 289)

P = pressure in millibars

T_v = virtual temperature in °Kelvin

and [23]

$$T_v = \frac{T}{1 - 0.379\left(\frac{e}{P}\right)} \tag{31}$$

where T is temperature in degrees Kelvin, and e is the partial pressure of the water vapor in the air (in millibars) given by

$$e = \frac{R_h}{100}(6.11)\,10^{\frac{7.5\,(T - 273.15)}{237.3 + (T - 273.15)}} \tag{32}$$

and R_h is the relative humidity in percent.

*The expression for g(h) is

$$g(h) = \frac{g_o r_o^2}{(r_o + h)^2} \text{ (meters/second}^2\text{)}$$

where the local acceleration of gravity g_o ([24], p. 488) and the effective earth's radius r_o ([24], p. 218) are functions of latitude ϕ_L.

$$g_o = 9.780356\,[1 + 0.0052885 \sin^2\phi_L - (5.9)10^{-6} \sin^2(2\phi_L)]$$

$$r_o = \frac{2g_o}{[(3.085462) \times 10^{-6} + (2.27) \times 10^{-9} \cos(2\phi_L) - 2 \times 10^{-12} \cos(4\phi_L)]}$$

It is sufficient to consider g(h) constant

$$g(h) \doteq G = 9.8 \text{ meters/second}^2 \tag{33}$$

Substituting (30) into (29), and using (28) and (31) gives

$$dP \doteq -\left(\frac{MG}{77.6R}\right)\left(\frac{T}{T_v}\right) N_d \, dh \tag{34}$$

Since we are assuming no water vapor, $e = 0$ and $(T/T_v) = 1$, and (34) becomes

$$dP \doteq -0.44 N_d \, dh \tag{35}$$

Integrating (35) gives

$$P = \int_P^\infty dP \doteq 0.44 \int_h^\infty N_d \, dh \tag{36}$$

Temperature T can now be obtained using (28) since N_d and P are known.

Base Temperature and Lapse Rate from Dry Refractivity

Equation (34) can be rewritten (again letting $(T/T_v) = 1$)

$$\frac{dP}{P} \doteq -\left(\frac{MG}{RT}\right) dh \tag{37}$$

Letting the temperature be linear with height, pressure can be obtained in closed form by integrating (37).

$$P = P_b \left(\frac{T}{T_b}\right)^{-\frac{MG}{R\beta}} \tag{38}$$

where T_b and P_b are the temperature and pressure respectively at the base $h = h_b$ of an atmospheric layer extending to some height h_T and β is the temperature lapse rate in that region. T is therefore given by

$$T = T_b + \beta(h - h_b) \quad \text{for} \quad (h_b \leq h \leq h_T) \tag{39}$$

Using (38) in (28) an expression for dry refractivity results.

$$N_d = N_b \left(\frac{T}{T_b}\right)^{-\left(\frac{MG}{R\beta} + 1\right)} \tag{40}$$

where N_b is the dry refractivity at the base $h = h_b$.

If temperature is constant with height between h_b and h_T, the corresponding expressions for P and N_d are

$$= P_b \exp\left[-\frac{MG}{RT_b}(h - h_b)\right] \tag{41}$$

and

$$N_d = N_b \exp\left[-\frac{MG}{RT_b}(h - h_b)\right] \quad \text{for} \quad (h_b \leq h \leq h_T) \tag{42}$$

From (41) and (42) it is seen that a constant temperature with height gives rise to an exponential distribution of pressure and an exponential refractivity profile.

Combining (40) and (42) results in an expression in two variables T_b and β for the ratio (N_d/N_b)

$$\frac{N_d}{N_b} = \begin{cases} \left[1 + \frac{\beta}{T_b}(h - h_b)\right]^{-\left(\frac{MG}{R\beta} + 1\right)} & \beta \neq 0 \\ \exp\left[-\frac{MG}{RT_b}(h - h_b)\right] & \beta = 0 \end{cases} \tag{43}$$

If three or more values of dry refractivity are available (two or more ratios), then least squares can be used to estimate T_b and β.

Apriori values for the base temperature $\tilde{T}_b$ and the lapse rate $\tilde{\beta}$ with weighting can be included in the least squares technique in the following way (these apriori values can be obtained from a standard atmosphere or previous measurements such as radiosonde data or satellite radiometer data).

Let w_{ai} represent the weights of the apriori values at the heights h_i and w_{oi} the weights of the corresponding recovered values for the ratios of the dry refractivity (N_i/N_o). Then the following sum of squares Q is to be minimized with respect to T_o and β.

$$Q = \sum_{i=1}^{m} w_{ai}^2 \left[F_i(\tilde{T}_o, \tilde{\beta}) - F_i(T_o, \beta)\right]^2 + w_{oi}^2 \left[(N_i/N_o - F_i(T_o, \beta)\right]^2 \tag{44}$$

where

$$F_i(T_o, \beta) = \begin{cases} \left[1 + \frac{\beta}{T_o}(h_i - h_o)\right]^{-\left(\frac{MG}{R\beta} + 1\right)} & \beta \neq 0 \\ \exp\left[-\frac{MG}{RT_o}(h_i - h_o)\right] & \beta = 0 \end{cases} \tag{45}$$

In (44) $\tilde{T}_o$ is an apriori estimate for the temperature at the height h_o, while T_o is the "solved for" value at h_o. $\tilde{T}_o$ is obtained from

$$\tilde{T}_o = \tilde{T}_b + \tilde{\beta}(h_o - h_b) \tag{46}$$

The Herglotz-Wiechert algorithm yields values of the refractive index (or equivalently refractivity) for corresponding values of the geocentric radius r. The underlying assumption in the method, however, is that refractivity is spherically symmetric (which follows from Snell's law). In order to obtain the height h_o in (44), the geocentric radius of the earth ρ_e for the closest point of approach of the ray connecting the two satellites must be known. As a good first approximation this can be obtained from some reference ellipsoid for the earth such as Fischer's model [25]

$$\rho_e = \frac{a_e\sqrt{1 - e^2}}{\sqrt{1 - e^2 \cos^2 \varphi'}} \tag{47}$$

where φ' = the geocentric latitude of the closest point of approach of the ray, and

$$e = \sqrt{2f - f^2} \tag{48}$$

where

$$(1/f) = 298.3$$

$$a_e = 6378.155 \text{ kilometers} \tag{49}$$

The height h_o is determined from

$$h_o = r_o - \rho_e \tag{50}$$

where r_o is one of the radii obtained by the inversion technique.

The value obtained for ρ_e from (47) does not represent the geoid surface (a surface of equal potential) exactly. However, a correction term can be added to ρ_e in (47) in order to more closely approximate the geoid surface [26].

It should be noted that although T_o and β are the parameters of a linear model for temperature, the least squares procedure is nonlinear in these variables. For computation purposes, a direct approach to solving for these parameters is to use a search technique to minimize Q in (44). This is not costly in terms of computation time inasmuch as there are only two parameters. In addition there is no need to calculate the partial derivatives.

Since any numerical procedure is subject to errors, both methods described above have certain limitations. With the numerical integration scheme a sufficient number of values of dry refractivity over a wide height range must be available to obtain pressure accurately. The main advantage, however, of

this method is that no assumptions are made concerning the temperature structure. On the other hand, if there are enough points in a given height range and an assumption of a linear temperature structure is not unreasonable, then least squares can be used to obtain the temperature profile. Instead of just one layer, the lower atmosphere could be broken up into two or more regions with differing lapse rates. This would, of course, necessitate more data points (values of dry refractivity).

9.0 ERROR ANALYSIS FOR RECOVERED PARAMETERS

In this section an error analysis is performed in order to assess the sensitivity of random and bias type errors on the recovered parameters. The error sources considered are measured range rate, position and velocity of the satellites (earth-fixed coordinate system), and height. For simplicity and ease of computation, an exponential model was chosen as the refractivity model for the lower atmosphere. It was felt that the errors from a more sophisticated model would be of the same order of magnitude for the same size error sources. The exponential model is given by

$$N_d = \exp(a_1 + a_2 s) \tag{51}$$

where $s = (0.01)h - 1$, h = height (kilometers), and $a_1 = -9.42$, $a_2 = -15.22$ km.

The nominal ephemeris used was an actual ephemeris of the ATS-6 and NIMBUS-6 satellites on 15 April 1976 [27].

Using Equations (1), (4), (24), and the model in (51), rays were traced between the positions of the satellites (as determined from the ephemeris) at five second intervals for a total of six data points. The range rate along the ray path was then calculated (from velocity components of the satellites) and served as a nominal "observable." The position and velocity components of the satellites were perturbed (either randomly or by adding a bias) and the parameters $\hat{a}_1$ and $\hat{a}_2$ solved for in the least square sense using the "observed" range rate and the perturbed ephemeris and employing ray trace procedures. In the case of simulated errors in the range rate, the perturbed range rate became the "observable" and the nominal ephemeris was used. Then, as before, $\hat{a}_1$ and $\hat{a}_2$ were solved for using least squares and ray tracing.

A Monte Carlo approach was used to simulate the effects of random errors in position, velocity, and range rate. A random sample of ten sets (each set containing six data points spaced five seconds apart) was used for the simulation and statistics taken on this sample. The standard deviations of the errors in position and velocity of each satellite were taken as being representative of ATS-6 and NIMBUS-6 short term accuracy [17]. In the case of position errors both satellite position components were perturbed and in the case of velocity errors both satellite velocity components were perturbed.

For any perturbed set of conditions, after solving for the parameters $\hat{a}_1$ and $\hat{a}_2$ in the least squares sense, there result errors Δa_1 and Δa_2 from the nominal conditions a_1 and a_2.

$$\Delta a_1 = \hat{a}_1 - a_1$$
$$\Delta a_2 = \hat{a}_2 - a_2 \qquad (52)$$

Neglecting for the moment errors in the height h, an error in N_d can be approximated by

$$\Delta N_d \doteq \left(\frac{\partial N_d}{\partial a_1}\right)\Delta a_1 + \left(\frac{\partial N_d}{\partial a_2}\right)\Delta a_2 \qquad (53)$$

or

$$\frac{\Delta N_d}{N_d} \doteq \Delta a_1 + s\Delta a_2 \qquad (54)$$

for bias type errors.

In the case of random errors, Δa_1 and Δa_2 are random variables and the variance of (54) becomes

$$\frac{\sigma^2_{\Delta N_d}}{N_d} \doteq \sigma^2_{\Delta a_1} + 2s\sigma_{\Delta a_1 \Delta a_2} + s^2\sigma^2_{\Delta a_2} \qquad (55)$$

where $\sigma^2_{\Delta a_1}$, $\sigma^2_{\Delta a_2}$, and $\sigma_{\Delta a_1 \Delta a_2}$ are the variances of Δa_1 and Δa_2 and the covariance between Δa_1 and Δa_2 which can be estimated from the sample.

Using (36) and (51) the pressure can be written as

$$P = \frac{-44}{a_2}\exp(a_1 + a_2 s) \qquad (56)$$

For pressure the following bias and random error expressions result.

$$\frac{\Delta P}{P} \doteq \Delta a_1 + \left(s - \frac{1}{a_2}\right) \Delta a_2 \tag{57}$$

and

$$\sigma^2_{\frac{\Delta P}{P}} \doteq \sigma^2_{\Delta a_1} + 2s\sigma_{\Delta a_1 \Delta a_2} + s^2 \sigma^2_{\Delta a_2} \tag{58}$$

For temperature, using (28) and (51)

$$T \doteq -\frac{3414.4}{a_2} \tag{59}$$

and therefore

$$\frac{\Delta T}{T} \doteq -\left(\frac{1}{a_2}\right) \Delta a_2 \tag{60}$$

and

$$\sigma^2_{\frac{\Delta T}{T}} \doteq \left(\frac{1}{a_2^2}\right) \sigma^2_{\Delta a_2} \tag{61}$$

for bias and random type errors respectively.

For errors in height, using (51) we can write

$$\frac{\Delta N_d}{N_d} \doteq (0.01)\, a_2\, \Delta h \tag{62}$$

and

$$\frac{\sigma^2_{\Delta N_d}}{N_d} \doteq 10^{-4}\, a_2^2\, \sigma^2_{\Delta h} \tag{63}$$

Since N is exponential, temperature is constant, and therefore there is no error with height.

Results of the error analysis can be seen in Figures 8 through 13. It is apparent from the figures that the percent error in recovered refractivity and pressure is linear with parameter error for a given height. Also, recovery of the parameters is more sensitive to errors in velocity of the satellites than to position errors, in particular, the position errors in the geostationary satellite.

It should be noted that the geoid varies approximately -110 to +80 meters over the globe with a standard error of about 5 meters from a reference ellipsoid [26]. Thus, using Equation (62) with an error of 5 meters and the value of a_2 as given in (51), recovered refractivity is in error less than 0.1%.

10.0 AN EXAMPLE

Figure 5 shows the lower atmospheric effect upon one-way range rate between the NIMBUS-6 satellite and the ATS-6 satellite on 15 April 1976. Radio occultation of the tracking signal between the two spacecraft occurred at about 20 hours, 47 minutes, 0 seconds GMT, and lasted for approximately half a minute. NIMBUS (in a near-circular almost polar orbit of 1100 kilometers height) was on a northern trajectory at about 64° South latitude and 116° West longitude while ATS was geostationary (equatorial plane) at 35° East longitude. The closest point of approach of the ray connecting the satellites was at 74° South latitude and 20° West longitude. The nearest radiosonde station at the approximate latitude was McMurdo Sound station located at $77^{\circ}\ 53^{m}$ South and $116^{\circ}\ 44^{m}$ East and the radiosonde data was taken at 0 GMT on 15 April 1976.

NIMBUS ACCURACY

x	15 meters	$\dot{x}$	5 cm/sec
y	10 meters	$\dot{y}$	3 cm/sec
z	20 meters	$\dot{z}$	8 cm/sec

ATS ACCURACY

x	50 meters	$\dot{x}$	0.2 cm/sec
y	50 meters	$\dot{y}$	0.2 cm/sec
z	50 meters	$\dot{z}$	0.5 cm/sec

RANGE RATE ACCURACY

0.5 cm/sec

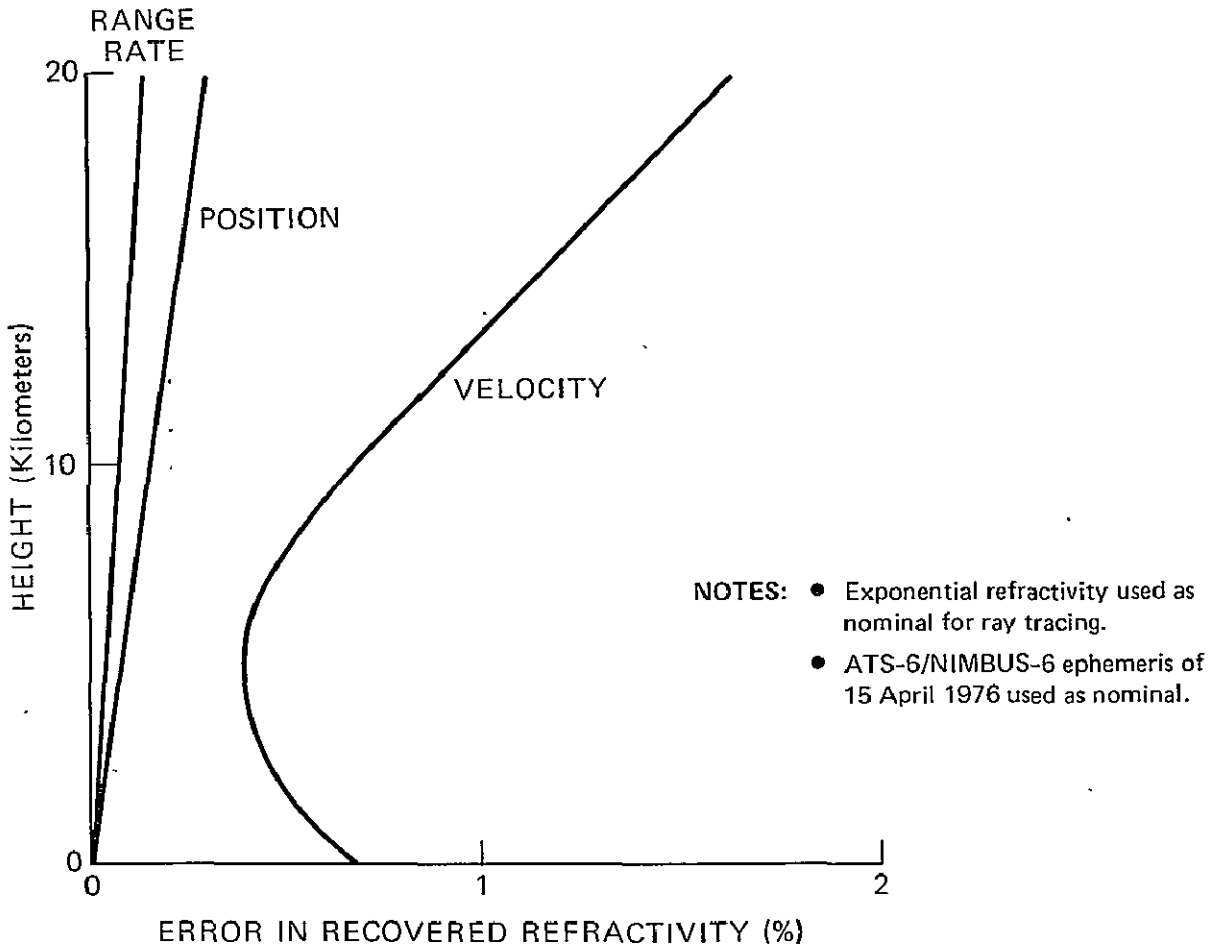

Figure 8. Effect of Random Errors on Recovered Refractivity (Monte Carlo)

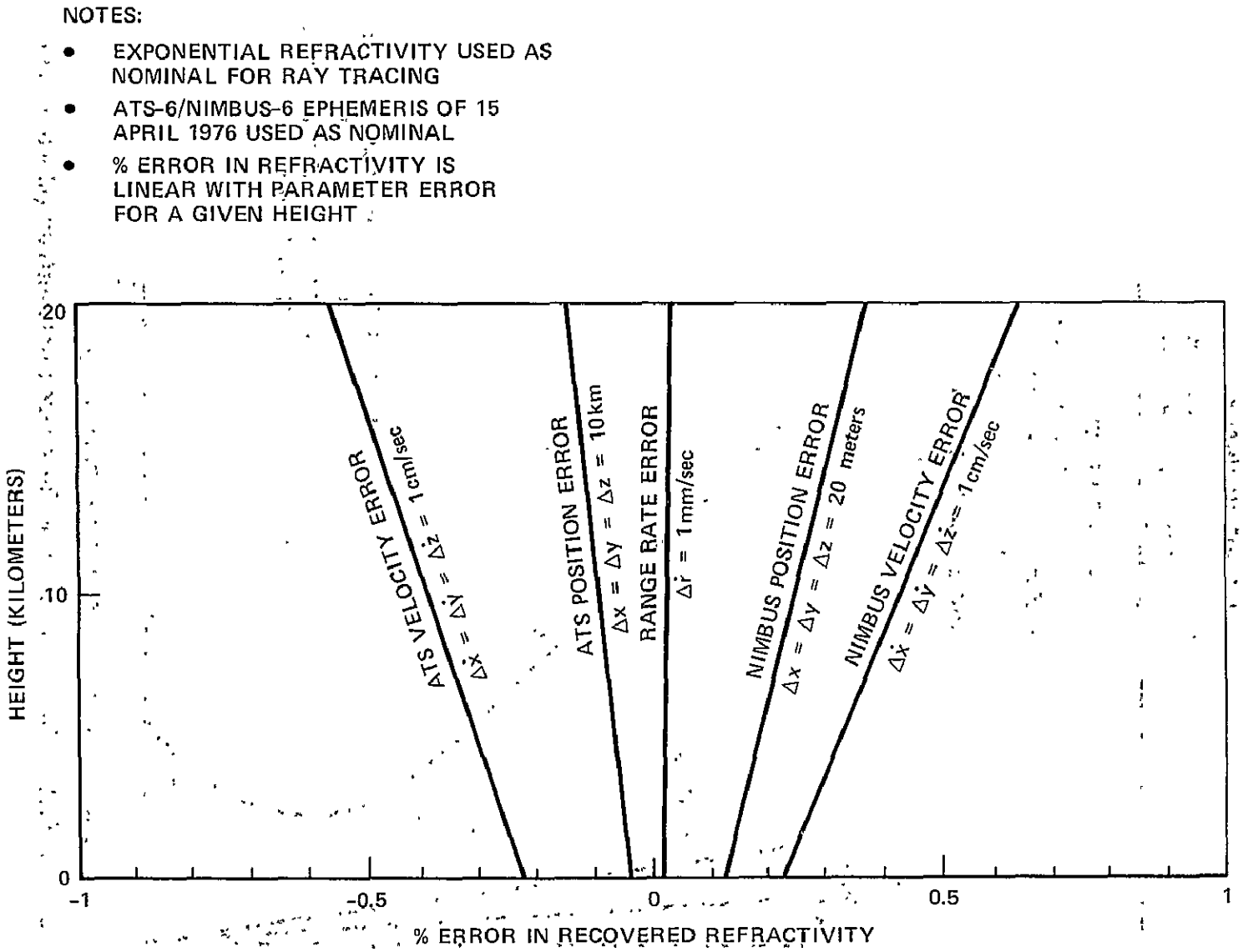

Figure 9. Effect of Bias Type Errors on Recovered Refractivity

NIMBUS ACCURACY

x	15 meters	$\dot{x}$	5 cm/sec
y	10 meters	$\dot{y}$	3 cm/sec
z	20 meters	$\dot{z}$	8 cm/sec

ATS ACCURACY

x	50 meters	$\dot{x}$	0.2 cm/sec
y	50 meters	$\dot{y}$	0.2 cm/sec
z	50 meters	$\dot{z}$	0.5 cm/sec

RANGE RATE ACCURACY

0.5 cm/sec

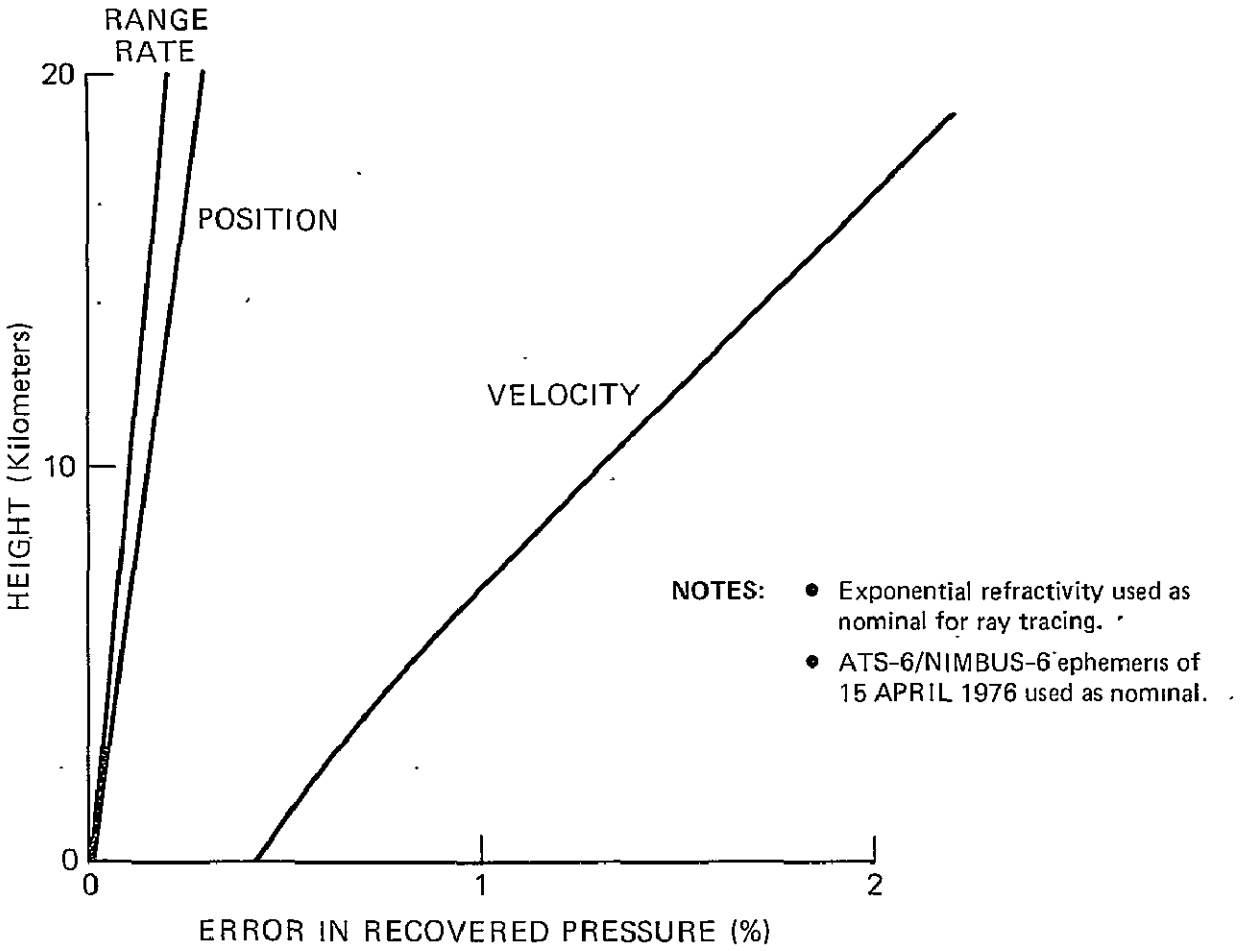

Figure 10. Effect of Random Errors on Recovered Pressure (Monte Carlo)

NOTES:

- EXPONENTIAL REFRACTIVITY USED AS NOMINAL FOR RAY TRACING
- ATS-6/NIMBUS-6 EPHEMERIS OF 15 APRIL 1976 USED AS NOMINAL
- % ERROR IN PRESSURE IS LINEAR WITH PARAMETER ERROR FOR A GIVEN HEIGHT

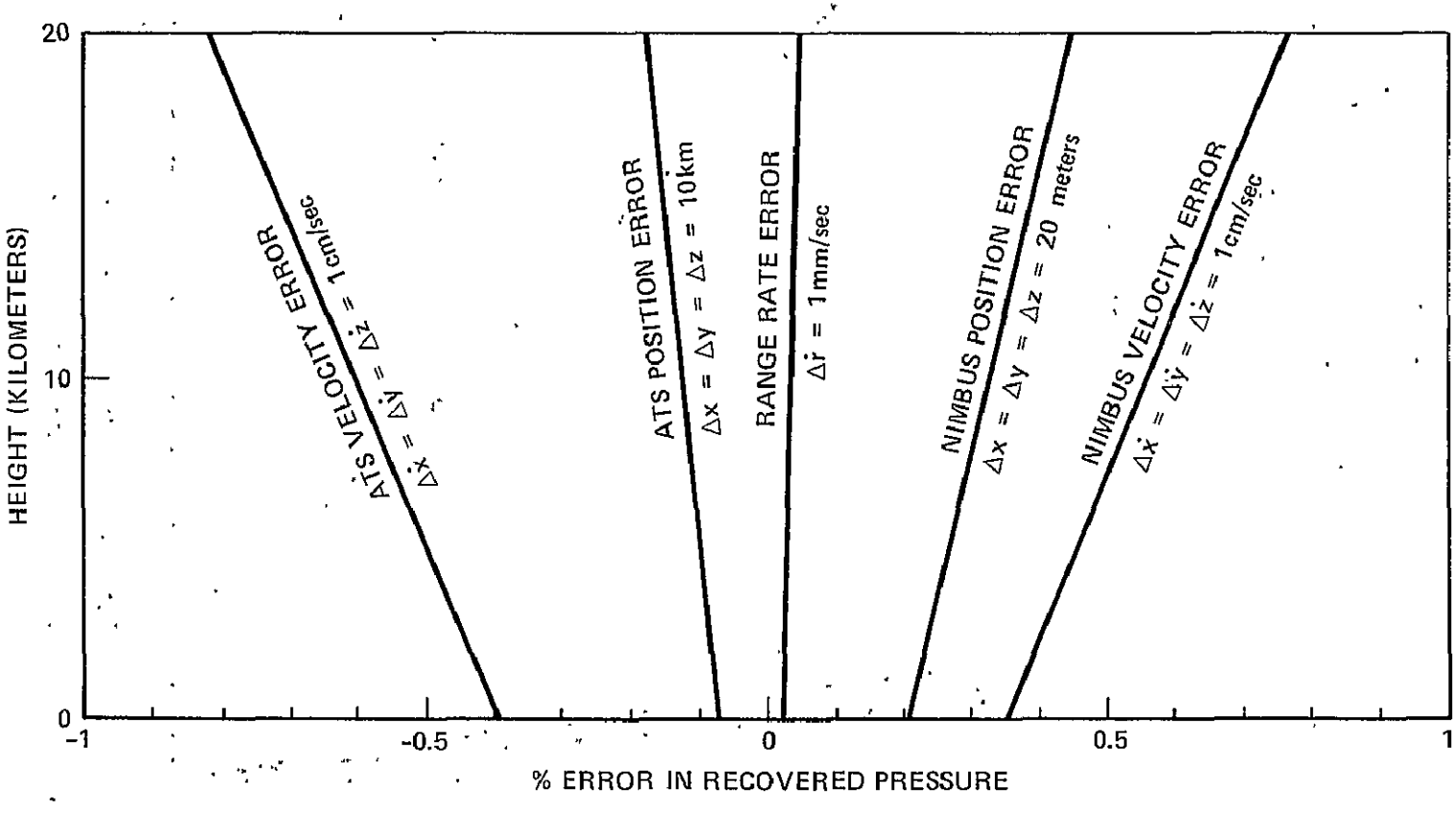

Figure 11. Effect of Bias Type Errors on Recovered Pressure

ERROR TYPE	% ERROR IN TEMPERATURE
Position	0.20
Velocity	0.68
Range Rate	0.05

NIMBUS ACCURACY

x - 15 meters	$\dot{x}$ - 5 cm/sec
y - 10 meters	$\dot{y}$ - 3 cm/sec
z - 20 meters	$\dot{z}$ - 8 cm/sec

ATS ACCURACY

x - 50 meters	$\dot{x}$ - 0.2 cm/sec
y - 50 meters	$\dot{y}$ - 0.2 cm/sec
x - 50 meters	$\dot{z}$ - 0.5 cm/sec

NOTES:

- Exponential refractivity used as nominal for ray tracing and therefore the nominal temperature distribution is a constant for all heights.
- ATS-6/NIMBUS-6 ephemeris of 15 April 1976 used as nominal.

Figure 12. Effect of Random Type Errors on Recovered Temperature (Monte Carlo)

ERROR SOURCE	% ERROR IN TEMPERATURE
NIMBUS POSITION $\Delta x = \Delta y = \Delta z = 20$ meters	-0.08
ATS POSTIION $\Delta x = \Delta y = \Delta z = 10$ kilometers	0.03
NIMBUS VELOCITY $\Delta \dot{x} = \Delta \dot{y} = \Delta \dot{z} = 1$ cm/second	-0.14
ATS VELOCITY $\Delta \dot{x} = \Delta \dot{y} = \Delta \dot{z} = 1$ cm/second	0.13
RANGE RATE $\Delta \dot{r} = 1$ mm/sec	-0.009

NOTES:

- EXPONENTIAL REFRACTIVITY USED AS NOMINAL FOR RAY TRACING AND THEREFORE THE NOMINAL TEMPERATURE DISTRIBUTION IS A CONSTANT FOR ALL HEIGHTS
- ATS-6/NIMBUS-6 EPHEMERIS OF 15 APRIL 1976 USED AS NOMINAL
- % ERROR IN RECOVERED TEMPERATURE IS LINEAR WITH PARAMETER ERRORS

Figure 13. Effect of Bias Type Errors on Recovered Temperature

The ephemeris of both satellites during occultation was obtained by propagating their state vectors at epoch [27] (a time point close to occultation) through this period of time. The states at epoch were determined from non-occulted tracking data. In the case of ATS-6 approximately 3300 observations of two-way range and range rate tracking measurements made from the Madrid tracking station at a data rate of one per ten seconds were used in the solution. For NIMBUS-6 about 2500 measurements of the 4-way range and range rate (see Section 4.0) from Madrid were used in the solution. An 8 x 8 gravity field for NIMBUS and a 4 x 4 gravity field for ATS were used also. Drag was not applied for either satellite. However, solar pressure was used in the solution for ATS-6 [27].

Refractivity was recovered using the ephemeris of the satellites and all but the last nine points of data in Figure 5 by the Herglotz-Wiechert direct integral transform technique and by a least squares procedure as a check. The last nine points of data (from 20 hours, 47 minutes, 25 seconds, to 20 hours, 47 minutes, 33 seconds) were excluded from the calculations as it was felt that these points were quite noisy, possibly due to loss of lock of the tracking signal or multipath effects or a combination of both.* Results of the recovered refractivity and refractivity calculated from radiosonde data are shown in Figure 14. Recovery by both methods differed by a maximum of about 2.3% at 10.5 kilometers.

Retrieval of pressure and temperature from dry refractivity was obtained by the two methods described in Section 8.0. Figure 15 shows pressure calculations against radiosonde. Direct integration of dry refractivity agreed more closely with radiosonde data with a maximum of about 3.5% at 10.5 kilometers. Temperature recovery is compared with radiosonde data in Figure 16. The solid line shows temperature for a standard atmosphere. Also shown are recovered temperature profiles using least squares with and without apriori weighting (the standard atmosphere was used as an apriori profile) and temperature obtained from dry refractivity and pressure (via numerical integration of

*When these points were included in the solution the resulting radii of closest approach of the ray connecting the two satellites did not decrease monotonically with time (i.e., as NIMBUS went below the horizon). This should occur for Snell's law to hold.

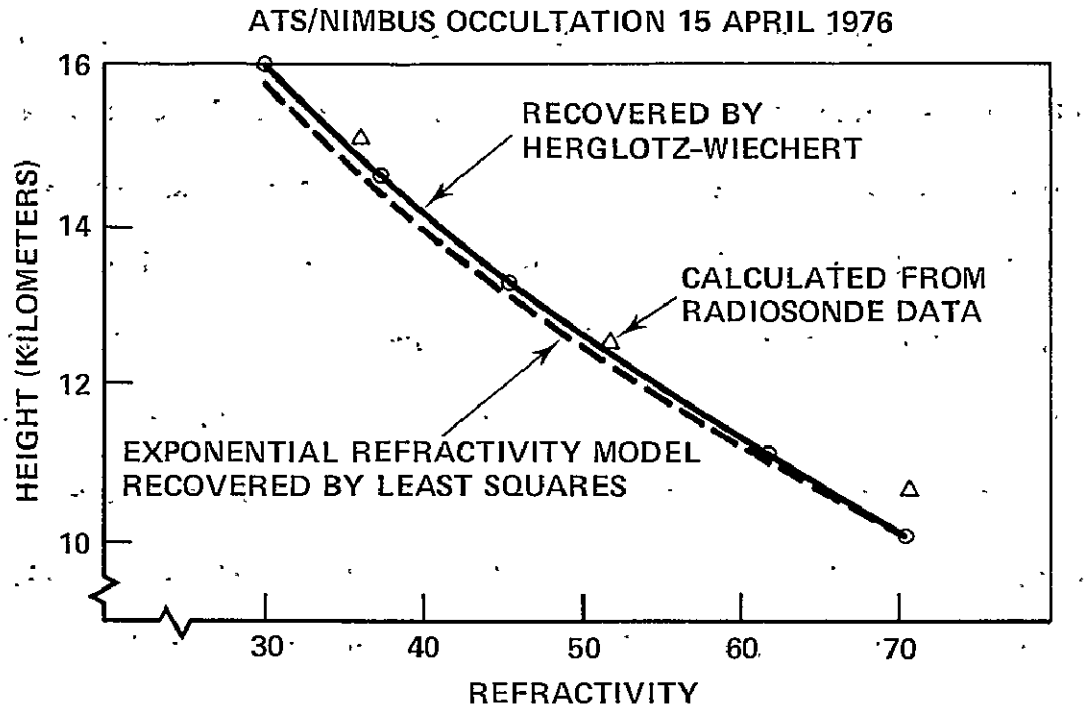

Figure 14. Comparison of Refractivity Recovery with Refractivity Calculated from Radiosonde Data

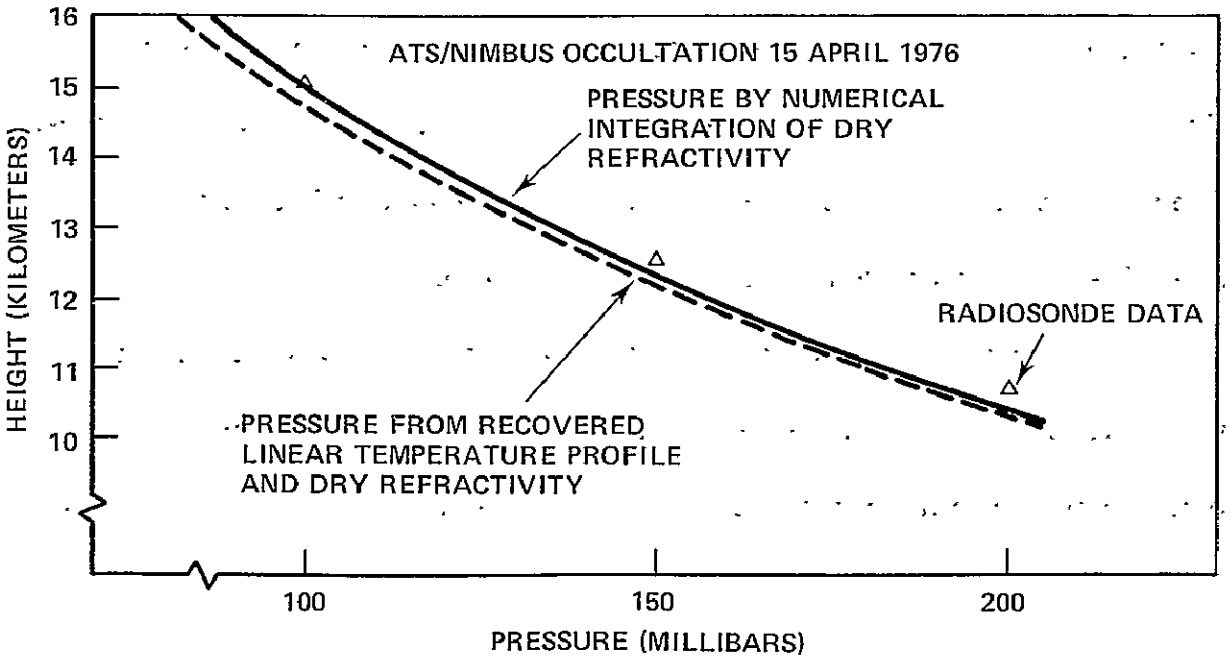

Figure 15. Pressure Recovery Versus Radiosonde Data

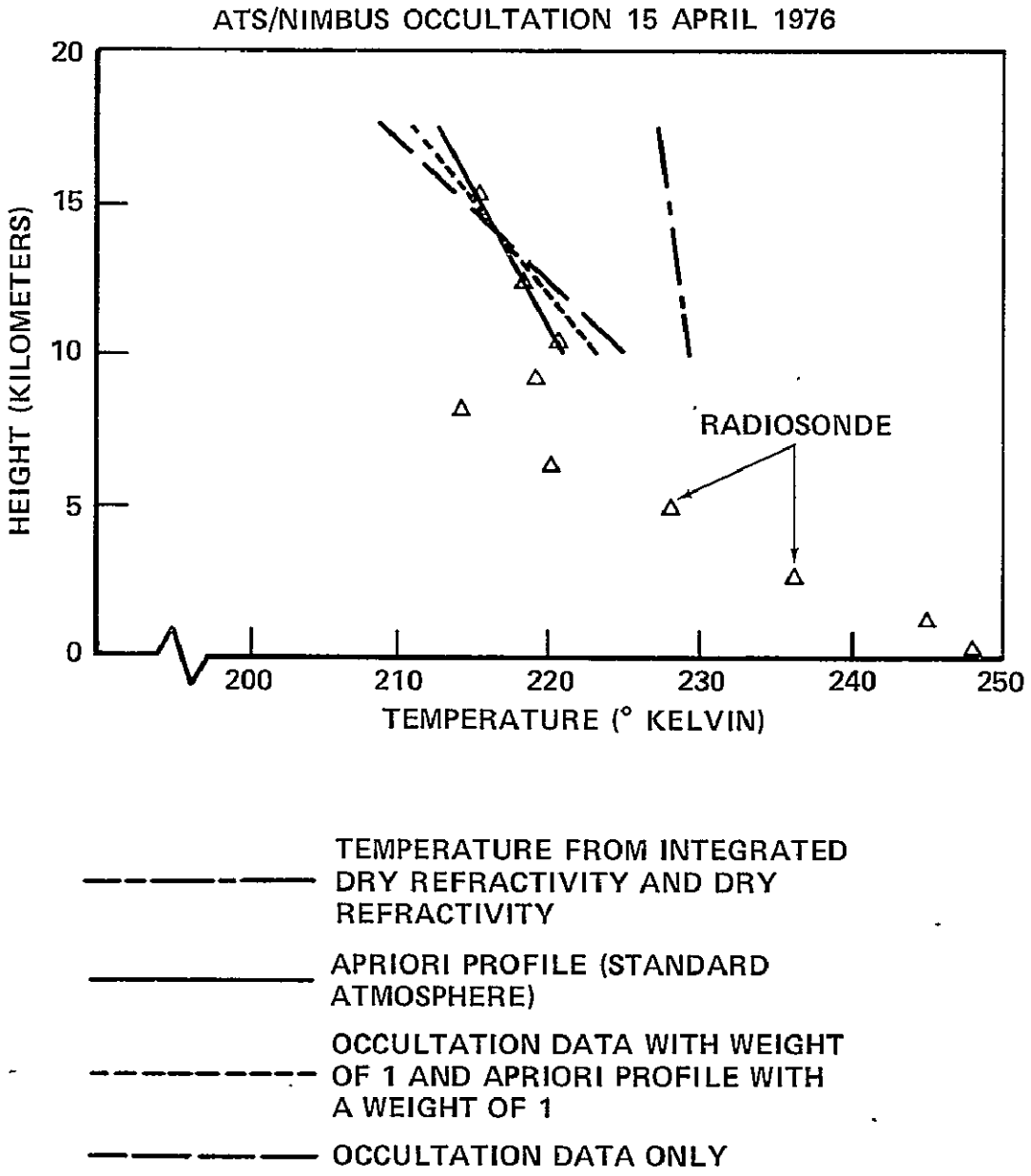

Figure 16. Temperature Recovery Versus Radiosonde Data

dry refractivity). Without weighting the maximum deviation of the least squares profile was 1.5% at 10.5 kilometers.

The radius of the geoid at the latitude and longitude of the point of closest approach of the ray was subtracted from the calculated radii of closest approach

using Fischer's model and a correction term for the geoid [26] to obtain height. Since the recovered data was at an altitude above 10 kilometers water vapor effects were not included. The local time of the pass was about 2 a.m. and therefore ionospheric effects were considered minimal and were not included.

11.0 DISCUSSION AND CONCLUSIONS

This analysis has demonstrated the feasibility of recovering refractivity profiles and pressure and temperature distributions for the lower atmosphere from radio occultation data taken during satellite-to-satellite tracking at S-band frequencies. One satellite, ATS-6, is in geostationary orbit (equatorial plane) and the other is in a near circular polar orbit. The only assumption made in the inversion technique is that refractivity is spherically symmetric (Snell's law holds).

Two methods have been investigated for determining pressure and temperature distributions from the recovered refractivity. In both methods it is assumed that the hydrostatic equation and perfect gas law hold. In a dry atmosphere refractivity is directly proportional to density, a function of both temperature and pressure. Using this fact, the first method consists of numerically integrating dry refractivity to obtain the pressure directly, without any assumptions concerning the temperature structure. Temperature can then be determined from pressure and dry refractivity. In the second method least squares is used to obtain the parameters of a linear temperature profile with height over a given region of the lower atmosphere (temperature at the base of the level and the

lapse rate in that region). Apriori information with appropriate weighting (such as a standard atmospheric temperature profile or previous radiosonde or satellite radiometer measurements) can be included. Pressure is then obtained from the recovered temperature profile and dry refractivity at the base of the layer. Both methods yield identical results for a linear temperature profile in a dry atmosphere.

At low altitudes the effects of water vapor in the atmosphere must be taken into account, either by independent measurement or by regression techniques using some assumed model [18]. At these altitudes and particularly at S-band frequencies (the carrier frequency of the tracking signal in this analysis is 2 GHz) ionospheric effects are almost negligible compared to lower atmospheric effects. At higher altitudes water vapor does not present a problem, but ionospheric effects increase somewhat. These effects can be removed by employing a dual frequency system. In the case of a single frequency system a simplified ionospheric model for electron density should suffice to remove these effects.

Results of an error analysis, where a simple exponential refractivity model for the lower atmosphere is assumed, indicate that recovery of atmospheric parameters is more sensitive to errors in the velocity components of the satellites than to errors in the position components of the satellites. This is particularly true for the geostationary satellite where a bias-type error as great as 10 kilometers in each of the position components gives rise to an error of less than 0.2% in

recovered refractivity up to approximately 20 kilometers. Errors in the velocity components of each satellite on the order of 1 centimeter/second give rise to errors less than 0.8% in pressure and refractivity and about 0.1% in temperature up to about 20 kilometers.

An example has been given demonstrating refractivity recovery and calculation of pressure and temperature distributions from radio occultation data obtained during satellite-to-satellite tracking of the NIMBUS-6 satellite (in near circular polar orbit) by the geostationary satellite ATS-6. An exponential refractivity profile was obtained by least squares procedures and used as a check against recovery by the Herglotz-Wiechert inversion algorithm. Recovery by both methods differed by a maximum of about 2.3% at a height of 16 kilometers. Both methods for calculating pressure and temperature were used and the results compared against radiosonde data. In the case of pressure recovery, direct integration of dry refractivity agreed more closely with radiosonde data with a maximum deviation of about 3.5% at 10.5 kilometers. The least squares procedure with and without apriori information yielded a temperature profile closer to the radiosonde data with a maximum deviation of about 1.5% at 10.5 kilometers.

With the geometrical configuration of the satellites as analyzed here, different levels of the atmosphere can be probed (as opposed to two satellites in the same orbit with a fixed spacing between them).

For a fixed inclination occultations will occur a few degrees in latitude below the value of inclination both in the northern and southern hemisphere. In addition the occultations will occur at different longitudes. For example, a satellite in a 1000 kilometer orbit about the earth will make about 14 revolutions per day which means 28 occultations at approximately the same latitude but varying longitudes. Thus, greater coverage could be accomplished by having a number of satellites at different inclinations. No additional electronic hardware (other than that required for satellite-to-satellite tracking) would be required onboard the spacecraft. The only requirement would be for the low satellite to be tracked as it went down or came up over the horizon with respect to the geostationary satellite at a sufficiently high data rate to ensure enough points for inversion procedures. Such a system could be used as an adjunct method for monitoring world-wide weather patterns.

REFERENCES

1. Schmid, P. E. and F. O. Vonbun, "The ATS-F/NIMBUS-F Tracking and Orbit Determination Experiment, 1974 IEEE INTERCON, New York City, March 26-29, 1974.

2. Colin, L., "Mathematics of Profile Inversion," Proceedings of Workshop Held at Ames Research Center, NASA TM X-62, 150, August 1972.

3. Kliore, Arvgdas, L. Cain, Gerald S. Levy, Von R. Eshleman, Gunnar Fjeldbo, and Frank D. Drake, "Occultation Experiment: Results of the

First Direct Measurement of Mars Atmosphere and Ionosphere," Science, Vol. 149, No. 3689, September 1965, pp. 1243-1248.

4. Fjeldbo, Gunnar, Weneke C. Fjeldbo, and Von R. Eshleman, "Models for the Atmosphere of Mars Based on Mariner 4 Occultation Experiment," J. Geophys. Res., Vol. 71, No. 9, May 1966, pp. 2307-2316.

5. Fjeldbo, Gunnar and Von R. Eshleman, "The Atmosphere of Mars Analyzed by Integral Inversion of the Mariner IV Occultation Data," Planet. Space Sci., Vol. 16, No. 8, August 1968, pp. 1035-1059.

6. Kliore, Rvgdas, Gerald S. Levy, Dan L. Cain, Gunner Fjeldbo, and S. I. Rasool, "Atmosphere and Ionosphere of Venus from the Mariner V S-Band Radio Occultation Measurement," Science, Vol. 158, No. 3809, December 1967, pp. 1683-1688.

7. Mariner Stanford Group: "Venus: Ionosphere and Atmosphere as Measured by Dual-Frequency Radio Occultation of Mariner V," Science, Vol. 158, No. 3809, December 1967, pp. 1678-1683.

8. Fjeldbo, G. and V. R. Eshleman, "Atmosphere of Venus as Studied with the Mariner V Dual Radio Frequency Occultation Experiment," Radio Science, Vol. 4, No. 10, October 1969, pp. 879-897.

9. Morrison, A. R., S. G. Ungar, and B. B. Lusignan, "An Occultation Satellite System for Determining Pressure Levels in the Atmosphere," Stanford Electronics Laboratories, NASA Langley Research Center, Contract NASA CR-132436, 1972.

10. Kliore, A., "Some Remarks on Meteorological Measurements with Occultation Satellites," Space Research IX, North-Holland Publishing Company, Amsterdam (1969).

11. Phinney, R. A., and D. L. Anderson, "On the Radio Occultation Method for Studying Planetary Atmospheres," Journal of Geophysical Research, Vol. 73, No. 5, March 1, 1968, pp. 1819-1827.

12. Bean, B. and E. Dutton, "Radio Meteorology," NBS Monograph 92, March 1, 1966.

13. Berry, F., E. Bollay, and N. Beers, "Handbook of Meteorology," McGraw Hill, N.Y., 1945.

14. Smith, W. L., "An Iterative Method for Deducing Tropospheric Temperature and Moisture Profiles from Satellite Radiation Measurements," Monthly Weather Review, 95, 363, 1967.

15. Smith, W. L., "An Improved Method for Calculating Tropospheric Temperature and Moisture from Satellite Radiometer Measurements," Monthly Weather Review, 96, 387, 1968.

16. Rodgers, C. D., "Retrieval of Atmospheric Temperature and Composition from Remote Measurements of Thermal Radiation," Reviews of Geophysics and Space Physics, Vol. 14, No. 4, November 1976.

17. Vonbun, F. O., Argentiero, P. D., Schmid, P. E., "Orbital Determination Accuracies using Satellite-to-Satellite Tracking," GSFC X-932-77-189 (October 1977).

18. Murray, Jr., C. W. and S. Rangaswamy, "Recovery of Atmospheric Refractivity Profiles from Simulated Satellite-to-Satellite Tracking Data," X-932-75-168, GSFC, June 1975.

19. Marini, J. W., Memorandum to Dr. F. O. Vonbun, "ATS-NIMBUS Occultation Experiment," December 13, 1972.

20. Barton, D. K., "Report of Ad Hoc Panel on Electromagnetic Propagation," in National Academy of Sciences Final Report, National Academy of Sciences, February 1963.

21. Bean, B. R. and G. D. Thayer, "Models of the Atmospheric Radio Refractive Index," Proc. of the IRE Vol. 47, May 1959, pp. 740-755.

22. Marini, J. W., Private Communication.

23. U.S. Standard Atmosphere Supplements, 1966, ESSA, NASA, USAF.

24. List, R. J., "Smithsonian Meteorological Tables," Sixth Revised Edition (Second Reprint), Publication 4014, 1963.

25. Mueller, I. I., "Spherical and Practical Astronomy as Applied to Geodesy," Fredenek Ungar Publishing Co., New York (1966).

26. Marsh, J. G., and F. E. Change, "Global Detailed Gravimetric Geoid," accepted for publication in Journal of Marine Geodesy (November 1977).

27. Guedney, V., Private Communication.

APPENDIX A

HERGLOTZ-WIECHERT INVERSION*

Referring to Figure 4, let r_0 be the radius of the outer limit of the atmosphere. Then, the electrical range from N (NIMBUS) to A (ATS) can be broken into three segments: the straight line distance outside the atmosphere from N to D, the electrical range along the ray path (inside the atmosphere) from D to B, and the straight line distance outside the atmosphere from B to A. The range from D to B is

$$R = 2\int_D^B n\,ds = 2\int_{r_p}^{r_o} n\left(\frac{dr}{\cos i}\right) \tag{A.1}$$

where $n = n(r)$ is the index of the refraction at radius r, i is the angle of incidence, ds is an incremental path length, and r_p is the radius of closest approach of the ray to the Earth.

Using Snell's law for a spherically stratified medium, a ray parameter p called the impact parameter is defined

$$p = n.r \sin i = r_o \sin i_o = n_p r_p \tag{A.2}$$

The parameter p is a constant along the ray path, and, in the absence of an atmosphere is the closest point of approach of the ray to the Earth.

*This derivation follows that in [11].

Defining a new variable η,

$$\eta = n\,r = \frac{p}{\sin i} \tag{A.3}$$

Equation (A.1) can be written

$$R = R(p) = 2\int_{p}^{r_o}\left(\frac{\eta^2}{r}\right)(\eta^2 - p^2)^{-1/2}\left(\frac{dr}{d\eta}\right)d\eta \tag{A.4}$$

Set

$$\begin{aligned} y &= \eta^2 - r_o^2 \\ w &= p^2 - r_o^2 \end{aligned} \tag{A.5}$$

Then (A.4) becomes

$$R(w) = -2\int_{o}^{w}(y + r_o^2)\left(\frac{d\ \ln r}{dy}\right)(y - w)^{-1/2}\,dy \tag{A.6}$$

In order to solve (A.6) for ln r the Abel transform pair is used

$$\begin{aligned} f(w) &= -k\int_{o}^{w} g'(y)\,(y - w)^{-1/2}\,dy \\ g(y) &= (k\pi)^{-1}\int_{o}^{y} f(w)\,(w - y)^{-1/2}\,dw \end{aligned} \tag{A.7}$$

Equation (A.6) is in the form of the first equation in (A.7) with $f = R$, $k = 2$, and

$$g'(y) = (y + r_o^2)\,\frac{d\ \ln r}{dy} \tag{A.8}$$

Differentiating the second equation in (A. 7) and changing back to the variables η and p

$$\eta^2\left\{\frac{d \ln r(\eta)}{d\eta}\right\} = \frac{d}{d\eta}\left\{(2\pi)^{-1/2}\int_{r_o}^{\eta} R(p)\,(p^2-\eta^2)^{-1/2}(2p)\,dp\right\} \tag{A.9}$$

Integrating (A. 9) from η to r_o

$$\ln\left(\frac{r(\eta)}{r_o}\right) = (-\pi)^{-1}\int_{\eta}^{r_o} u^{-2}\,(du)\,\frac{d}{du}\left\{\int_{r_o}^{u} R(p)\,(p^2-\eta^2)^{-1/2}\,(2p)\,dp\right\} \tag{A.10}$$

Integrating (A. 10) by parts gives

$$\ln\left(\frac{r(\eta)}{r_o}\right) = (-\pi)^{-1}\left(\frac{1}{\eta^2}\right)\int_{\eta}^{r_o} p\,R(p)\,(p^2-\eta^2)^{-1/2}\,dp + \left(\frac{2}{\pi}\right)\int_{\eta}^{r_o} u^{-3}\int_{u}^{r_o} p\,R(p)\,(p^2-u^2)^{-1/2}\,dp\,du \tag{A.11}$$

Interchanging the order of integration in the second term of (A. 11) gives

$$\left(\frac{2}{\pi}\right)\int_{\eta}^{r_o} u^{-3}\int_{u}^{r_o} p\,R(p)\,(p^2-u^2)^{-1/2}\,dp\,du$$

$$= \left(\frac{2}{\pi}\right)\int_{\eta}^{r_o} p\,R(p)\,dp\int_{\eta}^{p} u^{-3}\,(p^2-u)^{-1/2}\,du \tag{A.12}$$

$$= \left(\frac{2}{\pi}\right)\int_{\eta}^{r_o} p\,R(p)\left\{\frac{\sqrt{p^2-\eta^2}}{2p^2\eta^2} + \left(\frac{1}{2p^3}\right)\ln\left[\frac{p+\sqrt{p^2-\eta^2}}{\eta}\right]\right\}dp$$

Using

$$\cosh^{-1}(z) = \int_1^z (t^2 - 1)^{-\frac{1}{2}}\, dt = \ln\left[z + (z^2 - 1)^{\frac{1}{2}}\right] \tag{A.13}$$

the second term of (A.11) becomes

$$\left(\frac{2}{\pi}\right)\int_\eta^{r_o} u^{-3} \int_u^{r_o} p\,R(p)\,(p^2 - u^2)^{-\frac{1}{2}}\, dp\, du$$

$$= \left(\frac{1}{\eta^2\pi}\right)\int_\eta^{r_o} p\,R(p)\left[\frac{1}{p^2}\,(p^2 - \eta^2)^{\frac{1}{2}} + \left(\frac{\eta^2}{p^3}\right)\cosh^{-1}\left(\frac{p}{\eta}\right)\right] dp \tag{A.14}$$

Equation (A.10) can now be written

$$\ln\left(\frac{r(\eta)}{r_o}\right) = -\left(\frac{1}{\pi\eta^2}\right)\int_\eta^{r_o} p\,R(p)\left[(p^2 - \eta^2)^{-\frac{1}{2}} - \left(\frac{1}{p^2}\right)(p^2 - \eta^2)^{\frac{1}{2}} - \left(\frac{\eta^2}{p^3}\right)\cosh^{-1}\left(\frac{p}{\eta}\right)\right] dp$$

or

$$\ln\left(\frac{r(\eta)}{r_o}\right) = \frac{1}{\pi}\int_{r_o}^{\eta} R(p)\left\{\frac{1}{p\sqrt{p^2 - \eta^2}} - \left(\frac{1}{p^2}\right)\cosh^{-1}\left(\frac{p}{\eta}\right)\right\} dp \tag{A.15}$$

Using

$$\frac{d}{dp}\left\{\left(\frac{1}{p}\right)\cosh^{-1}\left(\frac{p}{\eta}\right)\right\} = -\left(\frac{1}{p^2}\right)\cosh^{-1}\left(\frac{p}{\eta}\right) + \left(\frac{1}{p}\right)\left(\frac{1}{\sqrt{p^2 - \eta^2}}\right) \tag{A.16}$$

and partial integration, Equation (A.15) is

$$\ln\left(\frac{r(\eta)}{r_o}\right) = -\frac{1}{\pi}\int_{r_o}^{\eta} \cosh^{-1}\left(\frac{p}{\eta}\right)\left(\frac{1}{p}\right)\left(\frac{d\Phi}{dp}\right) dp \tag{A.17}$$

At the closest point of approach of the ray r_p

$$r_p = r_o \exp\left\{-\frac{1}{\pi}\int_{r_o}^{\eta} \cosh^{-1}\left(\frac{p}{\eta}\right)\left(\frac{1}{p}\right)\left(\frac{dR}{dp}\right)dp\right\} \tag{A.18}$$

Using (A. 2)

$$n_p = \left(\frac{r_o \sin i_o}{r_p}\right) = (\sin i_o) \exp\left\{\frac{1}{\pi}\int_{r_o}^{\eta} \cosh^{-1}\left(\frac{p}{\eta}\right)\left(\frac{1}{p}\right)\left(\frac{dR}{dp}\right)dp\right\} \tag{A.19}$$

The range along the ray path from D to B, R, can be written as the sum of the range in the absence of an atmosphere, R_u, plus the range residual due to an atmosphere, R_a

$$R = R_u + R_a \tag{A.20}$$

In the absence of an atmosphere (A. 19) becomes

$$1 = (\sin i_o) \exp\left\{\frac{1}{\pi}\int_{r_o}^{\eta} \cosh^{-1}\left(\frac{p}{\eta}\right)\left(\frac{1}{p}\right)\left(\frac{dR_u}{dp}\right)dp\right\} \tag{A.21}$$

Substituting the expression for $\sin i_o$ obtained from (A. 21) into (A. 19) and using (A. 20) gives

$$n_p(\eta) = \exp\left\{-\frac{1}{\pi}\int_{\eta}^{r_o} \cosh^{-1}\left(\frac{p}{\eta}\right)\left(\frac{1}{p}\right)\left(\frac{dR_a}{dp}\right)dp\right\} \tag{A.22}$$

In the absence of an atmosphere

$$R_u = 2\,p \cot i_o \tag{A.23}$$

Therefore

$$R_a = R - R_u = 2 \int_{r_p}^{r_o} n \cdot d s - 2p \cot i_o \tag{A.24}$$

Using the electrical range from N to A and the fact that the range from N to D and the range from B to A are straight lines R_a can be written

$$R_a = R_e - \sqrt{R_A^2 - p^2} - \sqrt{R_N^2 - p^2} \tag{A.25}$$

where R_N and R_A are the radius vectors of the low and high satellites respectively.

Then, differentiating (A.25) gives

$$\frac{dR_a}{dp} = \dot{R}_e \left(\frac{dt}{dp}\right) + p[(R_A^2 - p^2)^{-1/2} + (R_N^2 - p^2)^{-1/2}] \tag{A.26}$$

The expression in (A.26) is used in (A.22) and contains the measured one-way range rate along the ray path from NIMBUS to ATS.

BIBLIOGRAPHIC DATA SHEET

1. Report No.	2. Government Accession No.	3. Recipient's Catalog No.
TM 78020		

4. Title and Subtitle	5. Report Date
Recovery of Refractivity Profiles and Pressure and Temperature Distributions in the Lower Atmosphere from Satellite-to-Satellite Radio Occultation Data	November 1977
	6. Performing Organization Code
7. Author(s)	8. Performing Organization Report No.
Charles W. Murray, Jr.	
9. Performing Organization Name and Address	10. Work Unit No.
GSFC (NASA) Greenbelt, Maryland	11. Contract or Grant No.
	13. Type of Report and Period Covered
12. Sponsoring Agency Name and Address	
	14. Sponsoring Agency Code

15. Supplementary Notes

To be published in Radio Science.

16. Abstract

This paper demonstrates the feasibility of recovering lower atmospheric refractivity profiles and retrieving certain atmospheric parameters such as temperature and pressure from satellite-to-satellite radio occultation data at S-Band frequencies.

The tracking data (one-way range rate) is inverted by an integral transformation (Abel transform) to obtain a vertical refractivity profile above the point of closest approach of the ray connecting the satellites. The only restriction concerning the refractivity is that it is spherically symmetric. After accounting for ionospheric and water vapor effects pressure and temperature are obtained from dry refractivity using the hydrostatic equation and perfect gas law.

An error analysis is performed to assess the sensitivity of random and bias errors upon recovered parameters.

An example is given using occultation data obtained during satellite-to-satellite tracking of the NIMBUS-6 spacecraft via the geostationary ATS-6 satellite.

17. Key Words (Selected by Author(s))	18. Distribution Statement
Occultation, Satellite-to-Satellite Tracking, Lower Atmosphere, Pressure, Temperature Refractivity	

19. Security Classif. (of this report)	20. Security Classif. (of this page)	21. No. of Pages	22. Price.*
None Unclass.	Unclass.		

*For sale by the National Technical Information Service, Springfield, Virginia 22151.